

Final Report for AOARD Grant #114108 (FA2386-11-1-4108)

**“Characterization of local carrier dynamics in AlN and AlGaN films using high spatial- and time-resolution cathodoluminescence spectroscopy”**

10/12/2012

**Principal Investigator:**

Shigefusa F. Chichibu, Dr. Eng. (Professor)  
Tohoku University  
Institute of Multidisciplinary Research for Advanced Materials (IMRAM)  
2-1-1 Katahira, Aoba, Sendai 980-8577, Japan  
Area Code/Phone Number: +81-22-217-5360      Fax Number: +81-22-217-5360  
E-mail: chichibu@tagen.tohoku.ac.jp

**Co-Principal Investigator:**

Kouji Hazu, Dr. Eng. (Assistant Professor, Chichibu Lab., Tohoku University, address the same as above)  
E-mail: k\_hazu@tagen.tohoku.ac.jp

Period of Performance: 08/22/2011 –08/21/2012

**Abstract:**

In order to assess the impacts of structural and point defects on the local carrier (exciton) recombination dynamics in wide bandgap AlN and high AlN mole fraction ( $x$ )  $\text{Al}_x\text{Ga}_{1-x}\text{N}$  films, high spatial- and time-resolution spatio-time-resolved cathodoluminescence (STRCL) measurement system was constructed by adopting a pulsed photoelectron (PE) gun that is excited using a femtosecond pulsed laser under a front-excitation configuration. The PE emission efficiency was increased by approximately an order of magnitude in comparison with that of the rear-excitation one. Accordingly, measurements of high signal-to-noise (S/N) ratio local cathodoluminescence (CL) spectra and time-resolved CL signals of AlN became possible. Another important achievement brought by the improved PE emission efficiency is that (S)TRCL measurement of slow decay components became possible, because the repetition rate of the excitation laser could be reduced using a pulse-picker (repetition rate reducer). Eventually, CL intensity mapping of the near-band-edge (NBE) emission of AlN became possible. We will use this STRCL system to correlate the radiative and nonradiative lifetimes with structural irregularities in the near future.

**Introduction:**

Aluminium nitride (AlN) and high AlN mole fraction  $\text{Al}_x\text{Ga}_{1-x}\text{N}$  alloys have attracted considerable interest for applications in UV-C (200~280 nm) DUV LEDs, because the bandgap energy ( $E_g$ ) of AlN is 6.01 eV at 300 K [1,2]. Taniyasu *et al.* have demonstrated [3] the shortest wavelength electroluminescence peak at 210 nm from an AlN *p-i-n* homojunction LED. However, its external quantum efficiency ( $\eta_{\text{ext}}$ ) was as low as  $10^{-8}$  [3], and the highest  $\eta_{\text{ext}}$  for the state-of-the-art AlGaN DUV LEDs is limited to be approximately 10% for the emission wavelength of 275 nm [4].

As known,  $\eta_{\text{ext}}$  is a product of internal quantum efficiency ( $\eta_{\text{int}}$ ), injection efficiency, and light extraction efficiency. The latter two components should be increased by optimizing device configurations and doping. Meanwhile,  $\eta_{\text{int}}$  is a material talent that is a fraction of radiative rate over the sum of radiative and nonradiative rates; *i. e.*  $\eta_{\text{int}} = (1 + \tau_R / \tau_{\text{NR}})^{-1}$ . To improve  $\eta_{\text{int}}$ ,  $\tau_R$  and  $\tau_{\text{NR}}$  must be quantitatively understood as functions of structural / point defect and impurity concentrations (crystal imperfections). However, only few papers [5-8] have dealt with the recombination dynamics of AlN and high- $x$   $\text{Al}_x\text{Ga}_{1-x}\text{N}$ , because of the lack of

## Report Documentation Page

*Form Approved*  
OMB No. 0704-0188

Public reporting burden for the collection of information is estimated to average 1 hour per response, including the time for reviewing instructions, searching existing data sources, gathering and maintaining the data needed, and completing and reviewing the collection of information. Send comments regarding this burden estimate or any other aspect of this collection of information, including suggestions for reducing this burden, to Washington Headquarters Services, Directorate for Information Operations and Reports, 1215 Jefferson Davis Highway, Suite 1204, Arlington VA 22202-4302. Respondents should be aware that notwithstanding any other provision of law, no person shall be subject to a penalty for failing to comply with a collection of information if it does not display a currently valid OMB control number.

1. REPORT DATE <b>23 JAN 2013</b>	2. REPORT TYPE <b>Final</b>	3. DATES COVERED <b>22-08-2011 to 21-08-2012</b>			
4. TITLE AND SUBTITLE <b>Characterization of local carrier dynamics in AlN and AlGaN films using high spatial- and time-resolution cathodoluminescence spectroscopy</b>		5a. CONTRACT NUMBER			
		5b. GRANT NUMBER			
		5c. PROGRAM ELEMENT NUMBER			
6. AUTHOR(S) <b>Chichibu Shigehide</b>		5d. PROJECT NUMBER			
		5e. TASK NUMBER			
		5f. WORK UNIT NUMBER			
7. PERFORMING ORGANIZATION NAME(S) AND ADDRESS(ES) <b>Tohoku University, Institute of Multidisciplinary Research for Advanced Material, 2-1-1 Katahira, Aoba, Sendai, Miyagi 980-8577, Japan, NA, NA</b>		8. PERFORMING ORGANIZATION REPORT NUMBER <b>N/A</b>			
9. SPONSORING/MONITORING AGENCY NAME(S) AND ADDRESS(ES) <b>AOARD, UNIT 45002, APO, AP, 96338-5002</b>		10. SPONSOR/MONITOR'S ACRONYM(S) <b>AOARD</b>			
		11. SPONSOR/MONITOR'S REPORT NUMBER(S) <b>AOARD-114108</b>			
12. DISTRIBUTION/AVAILABILITY STATEMENT <b>Approved for public release; distribution unlimited</b>					
13. SUPPLEMENTARY NOTES					
14. ABSTRACT <b>In order to assess the impacts of structural and point defects on the local carrier (exciton) recombination dynamics in wide bandgap AlN and high AlN mole fraction (x) Al<sub>x</sub>Ga<sub>1-x</sub>N films, high spatial- and time-resolution spatio-time-resolved cathodoluminescence (STRCL) measurement system was constructed by adopting a pulsed photoelectron (PE) gun that is excited using a femtosecond pulsed laser under a front-excitation configuration. The PE emission efficiency was increased by approximately an order of magnitude in comparison with that of the rear-excitation one. Accordingly, measurements of high signal-to-noise (S/N) ratio local cathodoluminescence (CL) spectra and time-resolved CL signals of AlN became possible. Another important achievement brought by the improved PE emission efficiency is that (S)TRCL measurement of slow decay components became possible, because the repetition rate of the excitation laser could be reduced using a pulse-picker (repetition rate reducer). Eventually, CL intensity mapping of the near-band-edge (NBE) emission of AlN became possible. We will use this STRCL system to correlate the radiative and nonradiative lifetimes with structural irregularities in the near future.</b>					
15. SUBJECT TERMS <b>Gallium Nitride , Spectroscopic Techniques, Time Resolved Cathodoluminescence Spectroscopy</b>					
16. SECURITY CLASSIFICATION OF:			17. LIMITATION OF ABSTRACT <b>Same as Report (SAR)</b>	18. NUMBER OF PAGES <b>25</b>	19a. NAME OF RESPONSIBLE PERSON
a. REPORT <b>unclassified</b>	b. ABSTRACT <b>unclassified</b>	c. THIS PAGE <b>unclassified</b>			



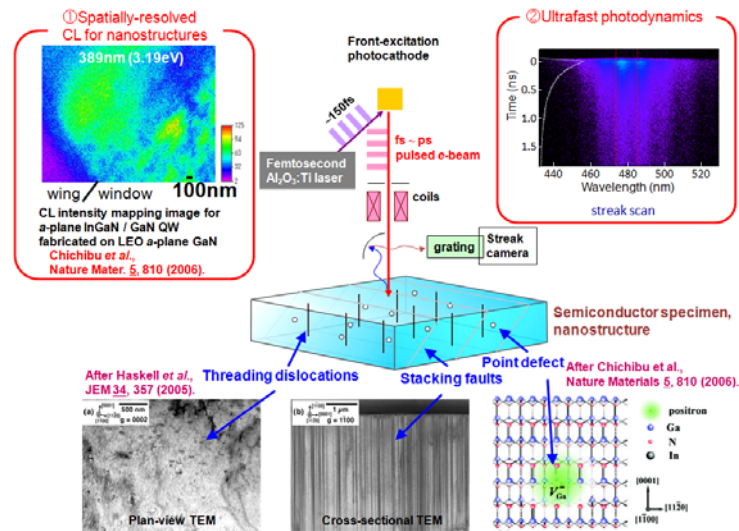


Fig. 1 Concept of the STRCL system equipped with a high emission efficiency front-excitation pulsed PE-gun. We will be able to correlate how structural defects influence the local CL lifetime, intensity, and wavelength.

a desirable DUV femtosecond excitation source.

In order to probe local carrier dynamics in wide  $E_g$  semiconductors, scanning near-field optical microscopy (SNOM) with a short-pulsed laser is widely used. On the other hand, the use of a scanning electron microscopy (SEM) equipped with a femtosecond PE-gun [7-14], namely STRCL technique [10-12,14], makes it possible to measure local TRCL signals at the positions defined precisely by the secondary electron (SE) image. This becomes attractive when characterizing very wide  $E_g$  materials such as AlN and  $\text{Al}_x\text{Ga}_{1-x}\text{N}$  alloys of high AlN mole fraction  $x$ . Indeed, STRCL takes full advantage of such a pulsed PE-beam, which enables high spatial resolution beyond the diffraction limit of light owing to the focused electronic excitation and thus makes it possible to interrogate local carrier/exciton dynamics. Unique opportunities offered by the STRCL demonstrated so far includes the investigations of the exciton dynamics around BSFs in an  $a$ -plane GaN [11], the exciton dynamics around the trapezoidal dimple surrounded by certain domain boundaries in a  $c$ -plane freestanding (FS-) GaN substrate [14], and the slight local variations of In incorporation in the  $\text{In}_{0.05}\text{Ga}_{0.95}\text{N}$  epilayer [12] grown on an  $m$ -plane FS-GaN. We have been using a rear-excitation configuration PE-gun [13], which was similar to that invented by EPFL group of Switzerland [9-12], for measuring STRCL data of above-mentioned  $c$ -plane FS-GaN substrate [14]. However, there remained several practical issues. One was the limited brightness of the photocathodes compared with conventional field emission (FE) sources, which made it difficult to acquire high magnification SEM images. The other was the decrease in PE intensity with time due to the driving damage of a 20-nm-thick *thin* Au film.

Here we report on significant improvement in the emission efficiency of our PE-gun, which enabled to measure high S/N ratio local CL spectra and TRCL signals of AlN. The higher efficiency PE-gun is excited using a femtosecond pulsed laser under a front-excitation configuration. Another important achievement was that (S)TRCL measurement of slow decay components became possible, because the repetition rate of the excitation laser can be reduced using a pulse-picker (repetition rate reducer), while keeping time-averaged PE number approximately the same for the SEM observation. Eventually, CL intensity mapping of the NBE emission of AlN became possible. We will use this STRCL system to correlate the radiative and nonradiative lifetimes with structural irregularities in the near future.

### Experiment:

Schematic diagram of the STRCL system equipped with the front-excitation configuration in-house PE-gun is shown in Fig. 2. It is principally the same as that used in Refs. [14] and

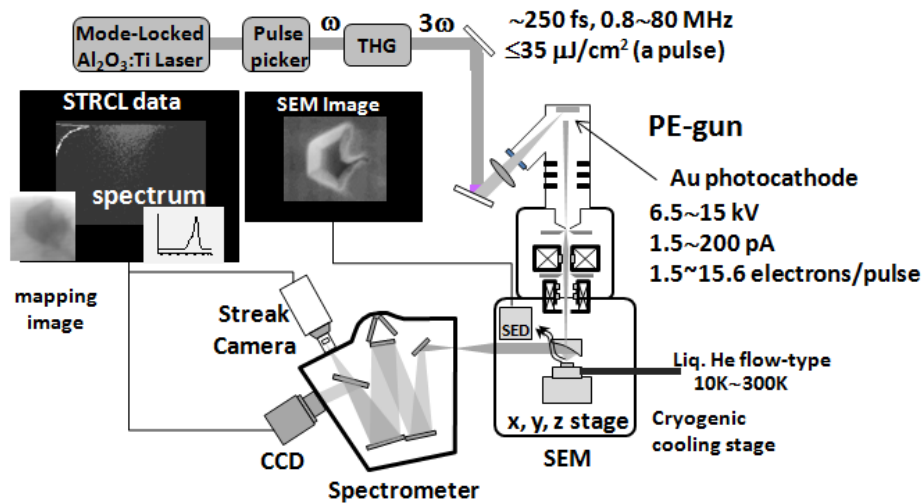


Fig. 2. Schematic diagram of our STRCL measurement system. The wavelength and repetition rate of the frequency-tripled ( $3\omega$ ) femtosecond  $\text{Al}_2\text{O}_3:\text{Ti}$  laser are adjusted according to the purpose of the measurement.

[15] except for the PE-gun, which is driven by a frequency-tripled mode-locked  $\text{Al}_2\text{O}_3:\text{Ti}$  laser pulses. The beam was focused using a fused silica lens with a spot diameter of  $50\ \mu\text{m}$  to a front-side of a photocathode. We note that we quit testing a field emission (FE)-type PE-gun that has been proposed in our workplan, because much simpler front-excitation configuration gun showed excellent PE emission performance, which will be described in the next section. The output  $e$ -beam was launched to the SEM by focusing it to its filament position. The probe current was calibrated using a Faraday cup placed just above the temperature-controlled stage, and was controllable between 0.1 and 200 nA at an acceleration voltage ( $V_{\text{acc}}$ ) of 12 kV by changing the average power of the excitation laser fluence. The luminescence from a sample was collected using an off-axis parabolic mirror ( $R=12\ \text{mm}$ ) placed above the sample and then analyzed using a grating spectrometer equipped with an electronically-cooled charged-coupled device and a streak camera with a temporal resolution of approximately 10 ps.

The standard sample measured in this work was an approximately  $2\text{-}\mu\text{m}$ -thick high quality (HQ)  $c$ -plane AlN epilayer grown on  $c$ -plane  $\text{Al}_2\text{O}_3$  by low-pressure metalorganic vapor phase epitaxy (MOVPE) [16,17]. The threading dislocation density (TDD) was  $2\times 10^8\ \text{cm}^{-2}$ , and it exhibited an atomically smooth surface with 0.25-nm-high monolayer atomic steps [16]. For quantifying the spatial resolution of the STRCL system, approximately  $500\text{-}\mu\text{m}$ -thick  $c$ -plane FS-GaN substrate was also measured [14]. Its TDD was estimated from the full-width at half-maximum (FWHM) values of the x-ray rocking curves (XRCs) using the relation given in Ref. [18]. Those containing edge components ( $N_{\text{E}}$ ) were estimated to be  $6.6\times 10^6\ \text{cm}^{-2}$ . Details of the growth [19,20] and fundamental optical properties [21] have been given in literatures.

## Results and Discussion:

### A. Improvements in PE emission efficiency by the use of a front-excitation configuration PE-gun

Figure 3 compares the measured PE current as a function of excitation laser power for the front-excitation and rear-excitation configuration PE-guns. For this experiment, the same 20-nm-thick Au-film was excited from either rear- or front-side for clarity, although much thicker bulk Au layer is preferable for a front-excitation PE-gun to get rid of the irradiation damage [22]. As shown, PE current was increased by an order of magnitude by the use of front-excitation configuration. The result means that both the quality of SEM images and S/N ratio of cw CL spectra will be improved: to obtain high-resolution SEM image, enough amount

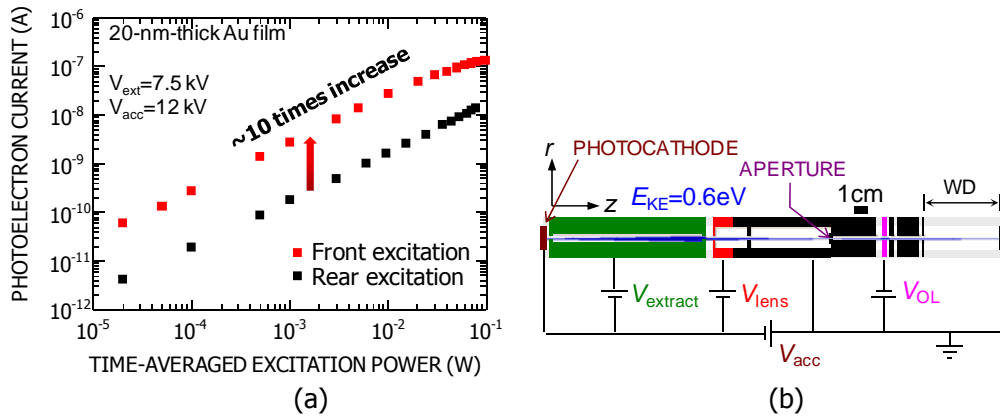


Fig. 3. (a) Photoelectron current as a function of time-averaged excitation laser power. The wavelength and repetition rate of the frequency-tripled ( $3\omega$ ) femtosecond  $\text{Al}_2\text{O}_3:\text{Ti}$  laser are adjusted according to the purpose of the measurement. (b) Schematic drawing [13] of the electron trajectory and the positions to give biases.

of secondary electrons (SEs) is required, meaning that bright PE source is advantageous. For measuring TRCL signals, we usually inject 1~1.5 electrons /pulse, in order to obtain the best temporal resolution. However, for measuring cw CL spectrum of better S/N ratio, the number of electrons should be increased properly.

### B. Local time-integrated and time-resolved CL signals of AlN

As the result of the increase in PE emission efficiency and well-focusing of the femtosecond  $e$ -beam pulse, we succeeded in improving three items.

(1) Obtained enough amount of PEs for measuring better S/N ratio time-integrated cathodoluminescence (TICL) spectra of AlN.

(2) Obtained well-focusing of the  $e$ -beam to excite  $e$ - $h$  pairs in a limited volume: we are able to reduce the number of electrons down to 1~1.5 per pulse, in order to prevent any degradation in temporal resolution [13]. The resultant number of excited  $e$ - $h$  pairs in AlN is deduced to be less than 1000 from the empirical relation given in Ref. [23].

(3) Obtained high PE emission efficiency to reduce the repetition rate of the excitation laser (and resultant  $e$ -beam) pulses, while keeping the quality of SEM pictures and TRCL decay curves.

Figure 4(a) shows a local TICL spectrum of the 2- $\mu\text{m}$ -thick  $c$ -plane AlN epilayer [7,16,17] measured at 15 K. The spectral lineshape is very similar to that measured with a wide-area cw excitation using the blanking technique, as shown in Fig. 4(b) (after Ref. [7]), although several

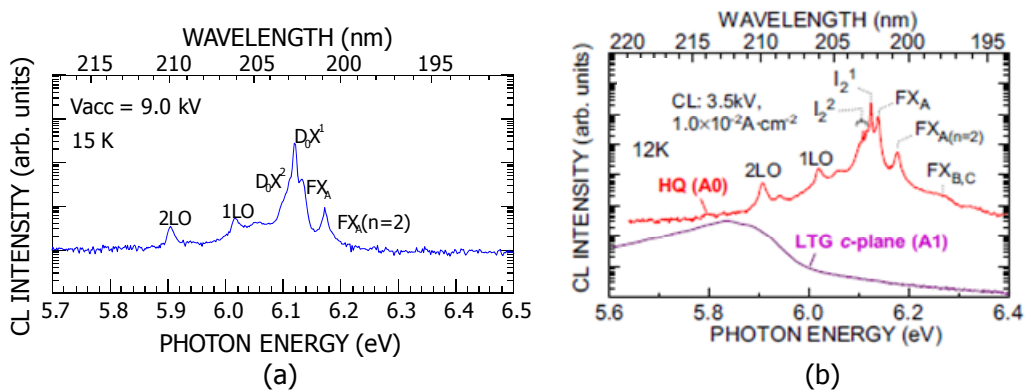


Fig. 4. (a) Very local TICL spectrum of a 2- $\mu\text{m}$ -thick  $c$ -plane AlN epilayer measured at 15 K. (b) Steady-state wide-area CL spectrum of the same HQ AlN epilayer (sample ID#A0) at 12 K (after Ref. [7]).

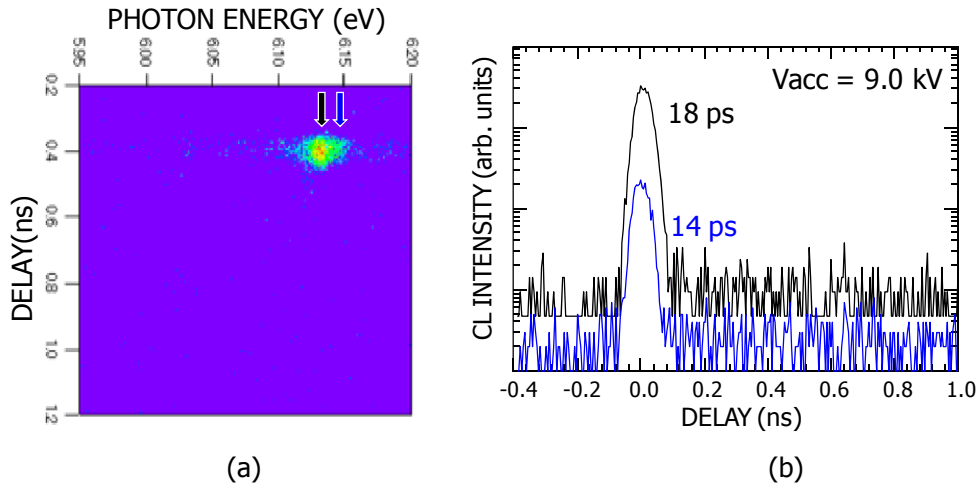


Fig. 5. (a) Very local streak-scope image showing the TRCL signal at 15 K for the *c*-plane AlN epilayer. (b) STRCL signals for  $D_0X^1$  (upper) and  $FX_A$  (lower) peaks measured for the photon energies marked in panel (a). We note that time-resolution of our STRCL system using the front-excitation configuration PE-gun is approximately 10 ps.

weak peaks/shoulders are absent probably due to the spatial inhomogeneity of the sample. We note that the peaks  $FX_A$ ,  $FX_{A(n=2)}$ ,  $D^0X^1$ ,  $D^0X^2$ , 1LO, and 2LO represent the emissions originating from the recombination of free A-excitons, recombination of the first excited state of free A-excitons, recombination of excitons bound to a neutral donor, recombination of excitons bound to another neutral donor, their 1-phonon replicas, and 2-phonon replicas, respectively. In Ref. [7],  $D^0X^1$  and  $D^0X^2$  are written as  $I_2^1$  and  $I_2^2$ , respectively.

In Fig. 5(a), local TRCL signal for the same *c*-plane AlN sample measured at 15 K is shown as a streak-scope image. As shown in Figs. 4(a) and 5(a), it is evident that we could monitor decay signals for  $D_0X^1$  and  $FX_A$ , as pointed by the arrows. Their emission wavelengths are approximately 203 and 202 nm, respectively. In the next stage we will use this STRCL system to correlate the radiative and nonradiative lifetimes with structural irregularities in AlN and  $Al_xGa_{1-x}N$  alloys of high *x*.

### C. Validation of the spatial resolution and the use of a pulse-picker for low repetition rate STRCL measurement

As listed in our achievements in section B.-(3), we reached sufficient PE emission efficiency for reduce the repetition rate of the excitation laser (and resultant *e*-beam) pulses, while keeping the quality of SEM pictures and TRCL decay curves. In addition, now we are able to measure much slower decay components, because the pulse interval can be adjusted from 12.5 ns to the longest limit of 125  $\mu$ s. This enabled us to measure long lifetimes for the NBE emission of an approximately 500- $\mu$ m-thick *c*-plane FS-GaN substrate [14]. Limitations for the spatial resolution of our STRCL-system and the relation between the room temperature internal quantum efficiency and nonradiative lifetime for the NBE emission of GaN are described in a paper listed in the Publication list a)-1). The paper is attached at the end.

### Summary and Prospects:

We constructed high spatial- and time-resolution STRCL measurement system by adopting a pulsed PE-gun excited using a femtosecond pulsed laser under a front-excitation configuration. The PE emission efficiency was increased by approximately an order of magnitude in comparison with that of the rear-excitation one. Accordingly, high S/N ratio local TICL spectra and TRCL signals of AlN were obtained. We will use this system to correlate the radiative / nonradiative lifetimes for the NBE excitonic emissions in wide AlN and high AlN mole fraction (*x*)  $Al_xGa_{1-x}N$  alloys with structural and point defects in the near future.

## References:

- [1] B. Gil, *Phys. Rev. B* **81**, 205201 (2010).
- [2] H. Ikeda, T. Okamura, K. Matsukawa, T. Sota, M. Sugawara, T. Hoshi, P. Cantu, R. Sharma, J. F. Kaeding, S. Keller, U. K. Mishra, K. Kosaka, K. Asai, S. Sumiya, T. Shibata, M. Tanaka, J. S. Speck, S. P. DenBaars, S. Nakamura, T. Koyama, T. Onuma, and S. F. Chichibu, *J. Appl. Phys.* **102**, 123707 (2007); erratum in *J. Appl. Phys.* **103**, 089901 (2008).
- [3] Y. Taniyasu, M. Kasu, and T. Makimoto, *Nature* **441**, 325 (2006).
- [4] M. Shatalov, W. Sun, A. Lunev, X. Hu, A. Dobrinsky, Y. Bilenko, J. Yang, M. Shur, R. Gaska, C. Moe, G. Garrett, and M. Wraback, *Appl. Phys. Express* **5**, 082101 (2012).
- [5] K. B. Nam, J. Li, M. L. Nakarmi, J. Y. Lin, and H. X. Jiang, *Appl. Phys. Lett.* **82**, 1694 (2003).
- [6] T. Onuma, K. Hazu, A. Uedono, T. Sota, and S. F. Chichibu, *Appl. Phys. Lett.* **96**, 061906 (2010).
- [7] S. F. Chichibu, T. Onuma, K. Hazu, and A. Uedono, *Appl. Phys. Lett.* **97**, 201904 (2010).
- [8] S. F. Chichibu, K. Hazu, T. Onuma, and A. Uedono, *Appl. Phys. Lett.* **99**, 051902 (2011).
- [9] M. Merano, S. Collin, P. Renucci, M. Gatri, S. Sonderegger, A. Crottini, J. D. Ganière, and B. Deveaud, *Rev. Sci. Instrum.* **76**, 085108 (2005).
- [10] M. Merano, S. Sonderegger, A. Crottini, S. Collin, P. Renucci, E. Pelucchi, A. Malko, M. H. Baier, E. Kapon, B. Deveaud, J. D. Ganière, *Nature* **438**, 479 (2005).
- [11] P. Corfdir, P. Lefebvre, J. Levrat, A. Dussaigne, J. -D. Ganière, D. Martin, J. Ristić, T. Zhu, N. Grandjean, and B. Deveaud-Plèdran, *J. Appl. Phys.* **105**, 043102 (2009).
- [12] M. Kagaya, P. Corfdir, J. -D. Ganière, B. Deveaud-Plèdran, N. Grandjean, and S. F. Chichibu, *Jpn. J. Appl. Phys.* **50**, 111002 (2011).
- [13] T. Onuma, Y. Kagamitani, K. Hazu, T. Ishiguro, T. Fukuda, and S. F. Chichibu, *Rev. Sci. Instrum.* **83**, 043905 (2012).
- [14] Y. Ishikawa, M. Tashiro, K. Hazu, K. Furusawa, H. Namita, S. Nagao, K. Fujito, and S. F. Chichibu, *Appl. Phys. Lett.* **101**, 212106 (2012).
- [15] S. F. Chichibu, Y. Ishikawa, M. Tashiro, K. Hazu, K. Furusawa, H. Namita, S. Nagao, K. Fujito, and A. Uedono, in press for *Electrochemical Society Transactions* (2013).
- [16] T. Shibata, K. Asai, S. Sumiya, M. Mouri, M. Tanaka, O. Oda, H. Katsukawa, H. Miyake, and K. Hiramatsu, *Phys. Status Solidi (c)* **0**, 2023 (2003).
- [17] T. Onuma, T. Shibata, K. Kosaka, K. Asai, S. Sumiya, M. Tanaka, T. Sota, A. Uedono, and S. F. Chichibu, *J. Appl. Phys.* **105**, 023529 (2009).
- [18] C. G. Dunn and E. F. Koch, *Acta Metal.* **5**, 548 (1957).
- [19] K. Fujito, S. Kubo, H. Nagaoka, T. Mochizuki, H. Namita, and S. Nagao, *J. Cryst. Growth* **311**, 3011 (2009).
- [20] K. Fujito, K. Kiyomi, T. Mochizuki, H. Oota, H. Namita, S. Nagao, and I. Fujimura, *Phys. Status Solidi A* **205**, 1056 (2008).
- [21] S. F. Chichibu, K. Hazu, Y. Ishikawa, M. Tashiro, H. Namita, S. Nagao, K. Fujito, and A. Uedono, *J. Appl. Phys.* **111**, 103518 (2012).
- [22] S. -S. Wellershoff, J. Hohlfeld, J. Güdde, and E. Matthias, *Appl. Phys. A* **69**, S99 (1999).
- [23] C. A. Klein, *J. Appl. Phys.* **39**, 2029 (1968).

## List of Publications and Significant Collaborations that resulted from your AOARD supported project:

- a) papers published in peer-reviewed journals,
  - 1) Y. Ishikawa, M. Tashiro, K. Hazu, K. Furusawa, H. Namita, S. Nagao, K. Fujito, and S. F. Chichibu, "Local lifetime and luminescence efficiency for the near-band-edge emission of freestanding GaN substrates determined using spatio-time-resolved cathodoluminescence", *Appl. Phys. Lett.* **101**, 212106 (2012).
- b) papers published in peer-reviewed conference proceedings,

none.

c) papers published in non-peer-reviewed journals and conference proceedings,  
none.

d) conference presentations without papers,

- 1) S. F. Chichibu, Y. Ishikawa, K. Hazu, M. Tashiro, K. Furusawa, H. Namita, S. Nagao, K. Fujito, and A. Uedono, "Spatio-time-resolved cathodoluminescence studies on freestanding GaN substrates grown by hydride vapor phase epitaxy", Pacific Rim Meeting on Electrochemical and Solid-State Science (PRiME 2012), Joint international meeting: 222nd Meeting of ECS, The Electrochemical Society and 2012 Fall Meeting of The Electrochemical Society of Japan, Session J3: Materials for Solid State Lighting, Hawaii Convention Center and the Hilton Hawaiian Village, Honolulu, Hawaii, USA, Oct. 7-12 (2012), No.J3-3956 (Invited-oral).
- 2) K. Furusawa, Y. Ishikawa, M. Tashiro, K. Hazu, S. Nagao, K. Fujito, A. Uedono, and S. F. Chichibu, "Local carrier dynamics in freestanding GaN substrates grown by hydride vapor phase epitaxy studied using the spatio-time-resolved cathodoluminescence technique", International Workshop on Nitride Semiconductors 2012 (IWN2012), Sapporo, Japan, Oct.14-19 (2012), No. MoP-GR-54 (poster).
- 3) S. F. Chichibu, Y. Ishikawa, M. Tashiro, K. Hazu, K. Furusawa, S. Nagao, K. Fujito, and A. Uedono, "Spatio-time-resolved cathodoluminescence study using a femtosecond focused electron beam on freestanding GaN substrates grown by hydride vapor phase epitaxy", The 39th International Symposium on Compound Semiconductors (ISCS 2012), Santa Barbara, CA, USA, Aug.27-30 (2012), No. We-2B.2 (oral).
- 4) S. F. Chichibu and A. Uedono, "Time-resolved luminescence studies on AlN and high AlN mole fraction AlGa<sub>N</sub> alloys", The Fourth International Symposium on Growth of III-Nitrides (ISGN-4), St. Petersburg, Russia, Jul.16-19 (2012), No. Th-1i (Invited-oral).

e) manuscripts submitted but not yet published,

- 1) S. F. Chichibu, T. Onuma, K. Hazu, and A. Uedono, "Time-resolved luminescence studies on AlN and high AlN mole fraction AlGa<sub>N</sub> alloys", Phys. Status Solidi (c) (2013) in press. This will be a peer-reviewed conference proceedings paper.
- 2) S. F. Chichibu, Y. Ishikawa, K. Hazu, M. Tashiro, K. Furusawa, H. Namita, S. Nagao, K. Fujito, and A. Uedono, "Spatio-time-resolved cathodoluminescence studies on freestanding GaN substrates grown by hydride vapor phase epitaxy", Electrochemical Society Transactions (to be published in 2013). This will be a peer-reviewed conference proceedings paper.

f) provide a list any interactions with industry or with Air Force Research Laboratory scientists or significant collaborations that resulted from this work.

We may interact with several researchers working on AlN and wide bandgap AlGa<sub>N</sub> materials in the future.

**Attachments:** Publications a) and e). **DD882:** is also attached.

# Local lifetime and luminescence efficiency for the near-band-edge emission of freestanding GaN substrates determined using spatio-time-resolved cathodoluminescence

Y. Ishikawa,<sup>1</sup> M. Tashiro,<sup>1</sup> K. Hazu,<sup>1</sup> K. Furusawa,<sup>1</sup> H. Namita,<sup>2</sup> S. Nagao,<sup>2</sup> K. Fujito,<sup>2</sup> and S. F. Chichibu<sup>1,a)</sup>

<sup>1</sup>Optoelectronics Laboratory, Institute of Multidisciplinary Research for Advanced Materials, Tohoku University, 2-1-1 Katahira, Aoba, Sendai 980-8577, Japan

<sup>2</sup>Gallium Nitride Department, Mitsubishi Chemicals Co., 1000, Higashi-mamiana, Ushiku, Ibaraki 300-1295, Japan

(Received 10 October 2012; accepted 29 October 2012; published online 21 November 2012)

Spatio-time-resolved cathodoluminescence measurements were carried out on low threading dislocation density freestanding GaN substrates grown by hydride vapor phase epitaxy. High-resolution cathodoluminescence imaging allows for visualization of nonradiative recombination channels in the vicinity of accidentally formed inversion domain boundaries. Local cathodoluminescence lifetimes ( $\tau_{CL}$ ) for the near-band-edge (NBE) emission are shown to be sensitively position dependent. A linear relation between the equivalent internal quantum efficiency ( $\eta_{int}^{eq}$ ) and  $\tau_{CL}$  for the NBE emission was observed at room temperature under a weak excitation condition, and spatially resolved excitation led to the observation of the highest  $\eta_{int}^{eq}$  of 20% with  $\tau_{CL}$  of 3.3 ns. © 2012 American Institute of Physics. [<http://dx.doi.org/10.1063/1.4767357>]

Wurtzite group-III nitride semiconductors have intensively been studied for the past few decades, and near-ultraviolet (UV) to green light emitting diodes (LEDs) as well as purple to blue laser diodes (LDs) based on InGaN active regions are now in common place.<sup>1,2</sup> Whilst InGaN LEDs fabricated on defective GaN templates grown on (0001) sapphire substrates, which have high density threading dislocations (TDs) typically  $10^8 \sim 10^9 \text{ cm}^{-2}$ , are commercially available owing to the defect-insensitive emission probability of InGaN alloys,<sup>3–6</sup> it becomes evident that high-quality GaN substrates are necessary not only for achieving ultimate performance and/or excellent reliabilities of optical devices but also for realizing AlGaIn/GaN power-switching transistors. For fabricating such substrates, hydride vapor phase epitaxy (HVPE) is one of the most commonly accepted techniques<sup>7</sup> despite cumulative bowing of the crystal plane that arises from the mismatch of the thermal expansion coefficients between GaN and the substrate used. Indeed, both *c*-plane and off-polar plane FS-GaN wafers with significantly reduced TD density ( $<10^7 \text{ cm}^{-2}$ ) and low basal-plane stacking fault (BSF) density ( $<10^3 \text{ cm}^{-1}$ ) are distributed.<sup>7,8</sup>

The internal quantum efficiency ( $\eta_{int}^{eq}$ ) for the near-band-edge (NBE) emission is determined by the balance between the radiative and the nonradiative recombination rates;  $\eta_{int}^{eq} = (1 + \tau_R/\tau_{NR})^{-1}$ , where  $\tau_R$  and  $\tau_{NR}$  are the radiative and nonradiative lifetimes, respectively. As  $\tau_{NR}$  for the NBE emission of GaN has been correlated with the gross concentration of point defects and complexes<sup>9</sup> rather than TD density, understanding local carrier (exciton) dynamics within low structural defect density areas of a GaN substrate is of paramount importance.

In order to probe local carrier dynamics in wide bandgap ( $E_g$ ) semiconductors, scanning near-field optical microscopy with a short-pulsed laser is widely used. However, use of a short-pulsed electron-beam (*e*-beam) (Refs. 10–15) becomes attractive when characterizing wide  $E_g$  materials such as AlN (Ref. 11). Spatio-time-resolved cathodoluminescence (STRCL) (Refs. 13–15) takes full advantage of such a pulsed *e*-beam, which enables high spatial resolution beyond the diffraction limit of light owing to the focused electronic excitation and thus makes it possible to interrogate local carrier/exciton dynamics. Unique opportunities offered by the STRCL demonstrated so far includes the investigations of the exciton dynamics around BSF in an *a*-plane GaN (Ref. 14) and the slight local variations of In incorporation in the  $\text{In}_{0.05}\text{Ga}_{0.95}\text{N}$  epilayer<sup>15</sup> grown on an *m*-plane FS-GaN.

In this letter, the correlation between the local cathodoluminescence (CL) intensities and lifetimes for the NBE emission is demonstrated using the STRCL technique in low TD density FS-GaN substrates grown by HVPE.<sup>7</sup> In the vicinity of an accidentally formed trapezoidal dimple surrounded by inversion domain boundaries (IDBs), the spatial variations of  $\tau_{CL}$  and carrier/exciton diffusion length ( $L_d$ ) are clearly visualized.

Approximately 0.5-mm-thick unintentionally doped *c*-plane FS-GaN substrates grown at 1050 °C using the vertical flow HVPE apparatus<sup>7</sup> were studied. The residual electron concentrations were  $3 \times 10^{18}$  and  $2 \times 10^{17} \text{ cm}^{-3}$  for samples A1 and A2, respectively. The TD densities were estimated from the full-width at half-maximum (FWHM) values of the x-ray rocking curves (XRCs) using the relation given in Ref. 16. Those containing edge components ( $N_E$ ) were estimated to be  $6.6 \times 10^6$  and  $6.3 \times 10^6 \text{ cm}^{-2}$  for A1 and A2, respectively.

Prior to STRCL measurement, macroarea steady-state photoluminescence (PL) and time-resolved photoluminescence (TRPL) measurements were carried out using the

<sup>a)</sup>Author to whom correspondence should be addressed. Electronic mail: chichibilab@yahoo.co.jp.

325 nm line of a cw He-Cd laser with an excitation intensity of  $20 \text{ W/cm}^2$  and a frequency-tripled mode-locked  $\text{Al}_2\text{O}_3 : \text{Ti}$  laser operating at a wavelength of 267 nm ( $200 \text{ nJ/cm}^2$ ), respectively. Note that for both cases, weak excitation conditions were maintained, meaning that the excited carrier concentration was lower than that of the residual carriers. Our STRCL system consists of a scanning electron microscope (SEM) equipped with an in-house photoelectron gun (PE-gun),<sup>12</sup> which was driven by a frequency-tripled mode-locked  $\text{Al}_2\text{O}_3 : \text{Ti}$  laser pulses. The beam was focused using a fused silica lens ( $f=300 \text{ mm}$ ) with a spot diameter of  $50 \mu\text{m}$  to a photocathode. The average power of 80 mW was used at a repetition rate of 80 MHz, corresponding to laser fluence of  $32 \mu\text{J/cm}^2$ . This value was limited by the onset of optical damage of the photocathode. The output  $e$ -beam was launched to the SEM by focusing it to its filament position. The probe current was calibrated by using a Faraday cup placed just above the temperature-controlled stage, and was typically 20 nA at an acceleration voltage ( $V_{acc}$ ) of 10 kV. Although this is smaller than what can be achieved with a conventional W filament, reasonable quality of SEM images can be obtained. The luminescence from a sample was collected using an off-axis parabolic mirror ( $R=12 \text{ mm}$ ) placed above the sample and then analyzed by using a grating spectrometer equipped with an electronically cooled charged-coupled device and a streak camera with a temporal resolution of approximately 10 ps.

Figure 1(a) shows a representative macroarea PL spectrum of A1 at 293 K. The sample exhibited a predominant NBE peak at 3.373 eV with the FWHM value of 73 meV and its LO phonon replica (a shoulder peak) at around 3.28 eV. The peak intensity of the broad emission band at around 2.2 eV (so-called yellow luminescence band) was more than three orders of magnitude lower than that of the NBE emission. The sample A2 showed an essentially same spectrum,

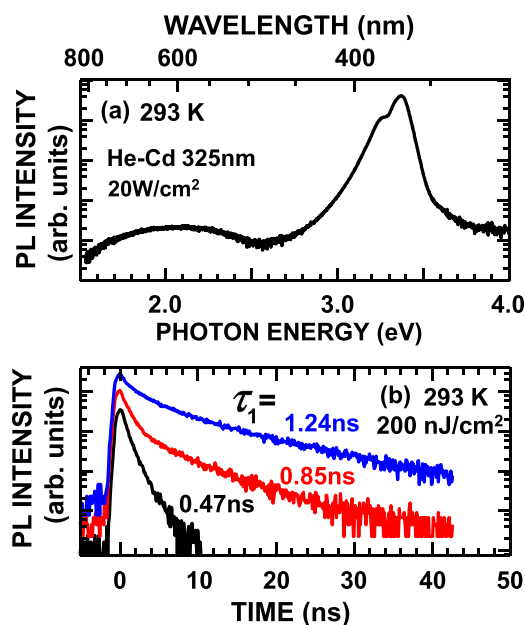


FIG. 1. (a) A macroarea steady-state PL spectrum at 293 K and (b) macroarea TRPL decay signals taken at 293 K for the NBE emission of the FS-GaN substrate grown by HVPE (A1). The TRPL signals were taken from three different positions, and vertical offsets are given for better looking.

indicating that both samples are of excellent quality. Figure 1(b) shows room temperature TRPL decay signals for the NBE emission in A1, measured at three different positions. It is found that characteristic lifetimes of the fast decay components ( $\tau_1$ ) were strongly position dependent, varying from 0.47 to 1.24 ns, although the overall PL spectra were almost unchanged (data not shown). The result implies that room temperature  $\tau_{NR}$  varies depending on the positions.

In order to visualize spatial variations of the luminescence intensity and to evaluate local  $\tau_{NR}$  for the NBE emission, STRCL measurement was conducted near the region surrounded by the IDBs in A1. We note that IDBs are occasionally formed by some growth perturbations. Figures 2(a)–2(c), respectively, illustrate SEM image and CL intensity images recorded for the NBE emission at 293 K and 20 K. These CL images were taken with a probe current of 100 pA and a dwell time of 200 ms, corresponding to 30 min per image. The SEM image showed a trapezoidal dimple surrounded by the IDBs. Also, several dark spots were found although their contrasts were rather faint. These spots were also observed as the dark spots in the CL image at 293 K, as shown in Fig. 2(b). The CL image at 293 K showed complex structures since its contrast reflects spatial distribution of nonradiative recombination centers (NRCs), while its spatial resolution is limited by  $L_d = \sqrt{D \cdot \tau}$  of minority carriers,<sup>17</sup> where  $D$  and  $\tau$  are their diffusivity and lifetime, respectively. The sharpness of the CL image taken at 20 K was greatly

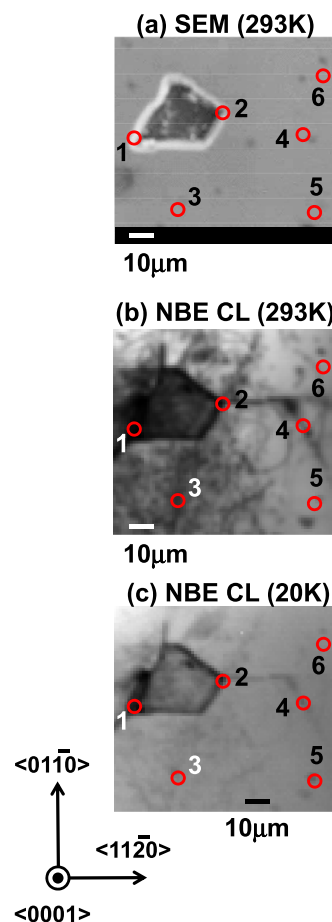


FIG. 2. (a) SEM image, (b) NBE CL intensity image taken at 293 K, and (c) NBE CL intensity image taken at 20 K for the FS-GaN sample A1.

improved because  $D$  approaches to zero towards 0 K according to Einstein's relation  $D = k_B T \mu / q$ , where  $k_B$  is the Boltzmann constant,  $T$  the temperature,  $q$  the electric charge, and  $\mu$  the mobility. Furthermore, since the NRCs are essentially frozen out at low temperatures, contributions from pure NRCs are excluded in Fig. 2(c). Therefore, the dark areas and lines that remain in Fig. 2(c) are possibly due to the absence of the material itself or the presence of extremely strong NRCs. In both Figs. 2(b) and 2(c), it can be seen that some straight line structures run from the corners of the trapezoid parallel to  $m$ -planes. This implies that the tensile stress accumulated around the IDBs is relaxed by introducing cracks. Since there are no corresponding structures in the SEM image, it is likely that these cracks run under the surface, and which can specifically be detected in the CL images due to the finite implantation depth of the  $e$ -beam and the longitudinal diffusion of the minority carriers.

The virtue of STRCL is that it is readily accessible to the local recombination dynamics for a particular emission peak. Local time-integrated cathodoluminescence (TICL) and time-resolved cathodoluminescence (TRCL) decay signals for the NBE emission of A1 measured at room temperature at the positions encircled in Fig. 2 are shown in Figs. 3(a) and 3(b), respectively. In this instance, the probe current was decreased to 25 pA, which amounts to 2 electrons per pulse, in order to prevent any degradation in temporal resolution.<sup>12</sup> The resultant number of excited electron-hole pairs in GaN is deduced to be less than 2000 from the empirical relation given in Ref. 18. We note that this excitation density gives the  $\tau_1$  value for the TRPL decay constant of a GaN template when excited with the laser fluence of  $2 \mu\text{J}/\text{cm}^2$  (Ref. 12). This value is an order of magnitude higher than that used for the TRPL measurement. However, weak excitation conditions are still maintained. The nominal NBE peak energy was approximately 3.38 eV, while the FWHM values were 90 meV, both of which are in reasonable agreement with Fig. 1(a). In these spectra, we found subtle redshifts of the NBE emission peak inside and on the peripheries of the trapezoid. This can be attributed to the local strain or increased residual electron concentration. We fit the decay curves by a double exponential function to extract  $\tau_1$ , and found that  $\tau_1$  significantly varied depending on

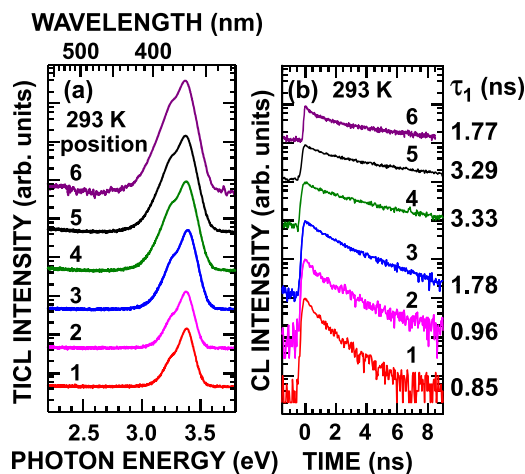


FIG. 3. Position dependent TICL spectra (a) and TRCL decay signals (b) for the NBE emission of FS-GaN sample A1 measured at 293 K. The number corresponds to the position encircled in Fig. 2.

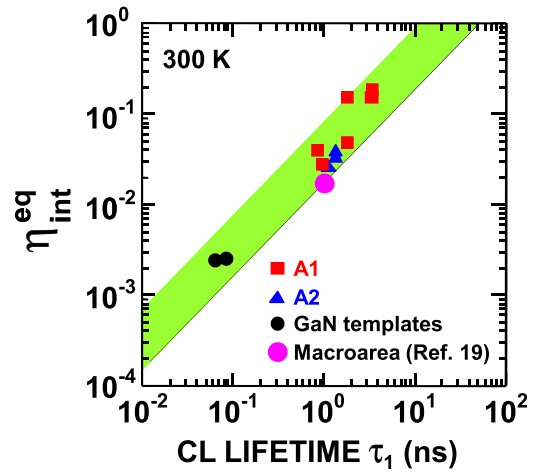


FIG. 4. The values of  $\eta_{int}^{eq}$  for the NBE emission peak of FS-GaN samples at room temperature as a function of the fast decay constant ( $\tau_1$ ) obtained from the STRCL measurement. The results for the macroarea measurement for both the HVPE FS-GaN (sample C0 in Ref. 19) that exhibited the longest positron diffusion length ( $L_+ = 116$  nm) and GaN templates are also included for reference.

the positions. The decrease of  $\tau_1$  near the visual defects in the CL image at 293 K [see Fig. 2(b)] can be understood as enhanced recombination at NRCs because  $\tau_1$  at room temperature is generally dominated by  $\tau_{NR}$ . By contrast, local  $\tau_1$  values measured at 10 K were almost independent of the positions being 180 ps. This is reasonable since  $\tau_R$  dominates  $\tau_{CL}$  at low temperature.

We also evaluated the local equivalent internal quantum efficiencies ( $\eta_{int}^{eq}$ ) for the NBE emission by simply taking the ratio of the integrated spectral intensities at 293 K to that at 20 K. The results for A1 and A2 are summarized as a function of  $\tau_1$  in Fig. 4. The best data for the macroarea PL measurement on similar HVPE FS-GaN (Ref. 19) and typical values observed for GaN templates are also plotted for reference. As shown,  $\eta_{int}^{eq}$  linearly increases with the increase in  $\tau_1$  according to  $\eta_{int}^{eq} = (1 + \tau_R/\tau_{NR})^{-1}$ , where we assume that  $\tau_R$  is an intrinsic value to a particular material<sup>20</sup> and that  $\tau_{CL}$  is generally dominated by  $\tau_{NR}$  at room temperature under the relation  $\tau_{CL}^{-1} = \tau_R^{-1} + \tau_{NR}^{-1}$ . Although the overall trend of higher  $\eta_{int}^{eq}$  in the local measurement may indicate somewhat higher excitation density used, the spatially focused excitation in STRCL can selectively probe highly luminescent regions that are less affected by NRCs. As a result, a record high  $\eta_{int}^{eq}$  of up to 20% was obtained for position 4 in Fig. 2, where  $\tau_1$  was as long as 3.33 ns.

In summary, local carrier recombination dynamics in the low TD density FS-GaN substrates grown by HVPE were studied by STRCL measurement. In addition to the visualization of defect networks originating from the IDBs in the CL intensity images, the spatially resolved TICL and TRCL measurements revealed a linear correlation between  $\eta_{int}^{eq}$  and  $\tau_{CL}$  at room temperature. The spatially focused excitation led us to observe the highest  $\eta_{int}^{eq}$  of 20% and the longest  $\tau_{CL}$  of 3.33 ns at 293 K. We believe that our results demonstrate the potential of FS-GaN grown by HVPE and serves as a benchmark for future development.

This work was supported in part by NEDO programs by METI and a Grant-in-Aids for Scientific Research Nos.

23645206 and 24760250 from MEXT, Japan, and AOARD/AFOSR monitored by Dr. G. Jessen.

- <sup>1</sup>S. Nakamura and G. Fasol, *The Blue Laser Diode: GaN Based Light Emitters and Lasers* (Springer, Berlin, 1997).
- <sup>2</sup>I. Akasaki and H. Amano, *Jpn. J. Appl. Phys.*, **36**, 5395 (1997).
- <sup>3</sup>S. F. Chichibu, T. Azuhata, T. Sota, and S. Nakamura, *Appl. Phys. Lett.* **69**, 4188 (1996); S. F. Chichibu, A. C. Abare, M. P. Mack, M. S. Minsky, T. Deguchi, D. Cohen, P. Kozodoy, S. B. Fleischer, S. Keller, J. S. Speck, J. E. Bowers, E. Hu, U. K. Mishra, L. A. Coldren, S. P. DenBaars, K. Wada, T. Sota, and S. Nakamura, *Mater. Sci. Eng., B* **59**, 298 (1999).
- <sup>4</sup>Y. Narukawa, Y. Kawakami, S. Fujita, S. Fujita, and S. Nakamura, *Phys. Rev. B* **55**, R1938 (1997).
- <sup>5</sup>L. Bellaiche, T. Mattila, L.-W. Wang, S.-H. Wei, and A. Zunger, *Appl. Phys. Lett.* **74**, 1842 (1999); P. R. C. Kent and A. Zunger, *ibid.* **79**, 1977 (2001).
- <sup>6</sup>S. F. Chichibu, A. Uedono, T. Onuma, B. A. Haskell, A. Chakraborty, T. Koyama, P. T. Fini, S. Keller, S. P. DenBaars, J. S. Speck, U. K. Mishra, S. Nakamura, S. Yamaguchi, S. Kamiyama, H. Amano, I. Akasaki, J. Han, and T. Sota, *Nature Mater.* **5**, 810 (2006).
- <sup>7</sup>K. Fujito, S. Kubo, H. Nagaoka, T. Mochizuki, H. Namita, and S. Nagao, *J. Cryst. Growth* **311**, 3011 (2009).
- <sup>8</sup>K. Fujito, K. Kiyomi, T. Mochizuki, H. Oota, H. Namita, S. Nagao, and I. Fujimura, *Phys. Status Solidi A* **205**, 1056 (2008).
- <sup>9</sup>S. F. Chichibu, A. Uedono, T. Onuma, T. Sota, B. A. Haskell, S. P. DenBaars, J. S. Speck, and S. Nakamura, *Appl. Phys. Lett.* **86**, 021914 (2005).
- <sup>10</sup>M. Merano, S. Collin, P. Renucci, M. Gatri, S. Sonderegger, A. Crottini, J. D. Ganière, and B. Deveaud, *Rev. Sci. Instrum.* **76**, 085108 (2005).
- <sup>11</sup>S. F. Chichibu, T. Onuma, K. Hazu, and A. Uedono, *Appl. Phys. Lett.* **97**, 201904 (2010).
- <sup>12</sup>T. Onuma, Y. Kagamitani, K. Hazu, T. Ishiguro, T. Fukuda, and S. F. Chichibu, *Rev. Sci. Instrum.* **83**, 043905 (2012).
- <sup>13</sup>M. Merano, S. Sonderegger, A. Crottini, S. Collin, P. Renucci, E. Pelucchi, A. Malko, M. H. Baier, E. Kapon, B. Deveaud, and J. D. Ganière, *Nature* **438**, 479 (2005).
- <sup>14</sup>P. Corfdir, P. Lefebvre, J. Levrat, A. Dussaigne, J.-D. Ganière, D. Martin, J. Ristić, T. Zhu, N. Grandjean, and B. Deveaud-Plédran, *J. Appl. Phys.* **105**, 043102 (2009).
- <sup>15</sup>M. Kagaya, P. Corfdir, J.-D. Ganière, B. Deveaud-Plédran, N. Grandjean, and S. F. Chichibu, *Jpn. J. Appl. Phys., Part 1* **50**, 111002 (2011).
- <sup>16</sup>C. G. Dunn and E. F. Koch, *Acta Metall.* **5**, 548 (1957).
- <sup>17</sup>K. Kumakura, T. Makimoto, N. Kobayashi, T. Hashizume, T. Fukui, and H. Hasegawa, *Appl. Phys. Lett.* **86**, 052105 (2005).
- <sup>18</sup>C. A. Klein, *J. Appl. Phys.* **39**, 2029 (1968).
- <sup>19</sup>S. F. Chichibu, K. Hazu, Y. Ishikawa, M. Tashiro, H. Namita, S. Nagao, K. Fujito, and A. Uedono, *J. Appl. Phys.* **111**, 103518 (2012).
- <sup>20</sup>D. Takamizu, Y. Nishimoto, S. Akasaka, H. Yuji, K. Tamura, K. Nakahara, T. Onuma, T. Tanabe, H. Takasu, M. Kawasaki, and S. F. Chichibu, *J. Appl. Phys.* **103**, 063502 (2008).

# Time-resolved luminescence studies on AlN and high AlN mole fraction AlGaN alloys

Shigefusa F. Chichibu<sup>\*,1</sup>, Takeyoshi Onuma<sup>1</sup>, Kouji Hazu<sup>1</sup>, and Akira Uedono<sup>2</sup>

<sup>1</sup> Institute of Multidisciplinary Research for Advanced Materials, Tohoku University, 2-1-1 Katahira, Aoba, Sendai 980-8577, Japan

<sup>2</sup> Division of Applied Physics, University of Tsukuba, 1-1-1 Tennodai, Tsukuba 305-8573, Japan

Received 9 September 2012, revised xx, accepted ZZZ

Published online ZZZ

**Keywords** deep ultraviolet, AlN, AlGaN, carrier dynamics, point defects, positron annihilation

\* Corresponding author: e-mail chichibulab@yahoo.co.jp, Phone: +81 22 217 5363, Fax: +81 22 217 5363

Impacts of point defects and impurities on the recombination dynamics for the near-band-edge (NBE) emission in AlN and high AlN mole fraction  $\text{Al}_x\text{Ga}_{1-x}\text{N}$  epilayers are revealed by means of deep ultraviolet (DUV) time-resolved luminescence and positron annihilation measurements. Extremely radiative nature of AlN is identified, as the radiative lifetime ( $\tau_R$ ) for a free excitonic polariton emission is as short as 10 ps at 7 K and 180 ps at 300 K, which are the shortest ever reported for spontaneous emission of bulk semiconductors. However,  $\tau_R$  increases with the increase in impurity and Al-vacancy ( $V_{\text{Al}}$ ) concentrations up to 530 ps at 7 K, irrespective of the threading dislocation (TD) density. Continuous decrease in  $\tau_R$  with temperature rise up to 200 K for heavily-doped

samples may reflect the carrier release from band-tail states. Similar to these AlN, low-temperature  $\tau_R$  for low-temperature-grown high- $x$   $\text{Al}_x\text{Ga}_{1-x}\text{N}$  are longer than that for low- $x$   $\text{Al}_x\text{Ga}_{1-x}\text{N}$ , AlN, or GaN due to the contribution of bound and localized tail-states. However,  $\tau_R$  shows little change with temperature rise, and is still a few ns at 300 K. The results essentially indicate an excellent radiative performance, although the luminescence efficiency of AlN and  $\text{Al}_x\text{Ga}_{1-x}\text{N}$  DUV light-emitting-diodes (LEDs) reported so far is limited by short nonradiative lifetimes ( $\tau_{\text{NR}}$ ). To increase  $\tau_{\text{NR}}$ , high temperature growth with appropriate defect management is preferable.

Copyright line will be provided by the publisher

**1 Introduction** Aluminium nitride (AlN) and high AlN mole fraction ( $x$ )  $\text{Al}_x\text{Ga}_{1-x}\text{N}$  alloys have attracted considerable interest for applications in UV-C (200~280 nm) DUV LEDs, because the bandgap energy ( $E_g$ ) of AlN is 6.01 eV at 300 K [1,2]. Taniyasu *et al.* [3] have demonstrated the shortest wavelength electroluminescence peak at 210 nm from an AlN *p-i-n* homojunction LED. However, its external quantum efficiency ( $\eta_{\text{ext}}$ ) was as low as  $10^{-8}$  [3], and typical  $\eta_{\text{ext}}$  for the state-of-the-art AlGaN DUV LEDs is approximately 3% [4].

As known,  $\eta_{\text{ext}}$  is a product of internal quantum efficiency ( $\eta_{\text{int}}$ ), injection efficiency, and light extraction efficiency. The latter two components should be increased by optimizing device configurations and doping. Meanwhile,  $\eta_{\text{int}}$  is a material talent that is a fraction of radiative rate over the sum of radiative and nonradiative rates; *i. e.*  $\eta_{\text{int}} = (1 + \tau_R / \tau_{\text{NR}})^{-1}$ . To improve  $\eta_{\text{int}}$ ,  $\tau_R$  and  $\tau_{\text{NR}}$  must be quantitatively understood as functions of structural / point defect and impurity concentrations (crystal imperfections). However, only few papers [5-8] have dealt with the re-

combination dynamics of AlN and high- $x$   $\text{Al}_x\text{Ga}_{1-x}\text{N}$ , because of the lack of a desirable DUV femtosecond excitation source.

In this article, the results of time-resolved luminescence and positron annihilation spectroscopy (PAS) measurements on AlN and high- $x$   $\text{Al}_x\text{Ga}_{1-x}\text{N}$  alloys are reported [6-8]. We first introduce two femtosecond excitation sources for time-resolved photoluminescence (TRPL) and time-resolved cathodoluminescence (TRCL) measurements. Then we quantify gross intrinsic  $\tau_R$  for a free excitonic polariton emission of high-quality AlN to identify its extremely radiative nature. Next we show the results for various quality AlN to reveal that point defects and impurities, rather than TDs, play the major role in limiting  $\tau_R$  and  $\tau_{\text{NR}}$  for the NBE emission. Finally, we show that  $\text{Al}_x\text{Ga}_{1-x}\text{N}$  epilayers of high  $x$  essentially have an excellent radiative performance.

## 2 Experimental procedures

Copyright line will be provided by the publisher

**2.1 Analytical techniques** Steady-state cathodoluminescence (CL) was excited using an electron beam ( $e^-$ -beam) operated at 3.5 kV acceleration voltage and  $1.0 \times 10^{-2}$  A·cm $^{-2}$  probe current density [6-9].

As  $E_g$  of AlN is as large as 6.01 eV [1,2], a frequency-quadrupled ( $4\omega$ ) mode-locked Al $_2$ O $_3$ :Ti laser [5-8] was used for the TRPL measurement. Approximately 115 fs pulses of the laser light (197~200 nm) were generated by mixing the fundamental ( $\omega$ ) and frequency-tripled ( $3\omega$ ) beams using a barium borate crystal, as shown in Fig. 1. The repetition rate and power density were 80 MHz and 40 nJ·cm $^{-2}$  (per pulse), respectively. The maximum electron-hole ( $e-h$ ) pair concentration is estimated to be  $4 \times 10^{15}$  cm $^{-3}$  during the pulse, assuming the absorption coefficient of AlN as  $10^5$  cm $^{-1}$  at 198 nm. In order to excite semiconductors having  $E_g$  larger than the photon energy of the  $4\omega$  beam, we constructed a femtosecond-laser-driven photoelectron gun (PE-gun) [7,8,10] similar to Ref. [11] for TRCL measurements. It consisted of a 15-nm-thick Au film, extraction electrodes, and acceleration electrodes to give  $V_{acc}$ , as shown in Fig. 1. The Au film was excited from the rear surface using the  $3\omega$  pulses of the Al $_2$ O $_3$ :Ti laser (240~280 nm, 100 fs,  $\sim 1$   $\mu$ J·cm $^{-2}$  a pulse). The distance between the PE-gun and the sample was 52.5 mm. The quantum efficiency of the PE-gun was approximately  $2.5 \times 10^{-6}$  electrons per photon for  $V_{acc}=10$  kV, and the  $e^-$ -beam current density was 1.8 pA·cm $^{-2}$  during each pulse. The corresponding excitation density calibrated to our TRPL is approximately 10 nJ·cm $^{-2}$ . Therefore, excitation intensities for TRPL and TRCL were low enough to satisfy a weak-excitation regime, which underlines the nonradiative processes at 300 K.

Energy-resolved TRPL and TRCL signals were acquired using a streak-camera, which limits the overall minimum time resolution approximately 7 ps. In case of TRCL, because  $e^-$ -beams can be implanted into far below the surface, unwanted surface recombination effects may be minimized. For example, the implantation depth profile peak is approximately 250 nm for  $V_{acc}=10$  kV. To systematically compare  $\tau_R$  and  $\tau_{NR}$  for various quality samples, the effective PL (CL) lifetime  $\tau_{PL(CL),eff}$  is defined [12] as the time after excitation when  $\int_0^{t_{lim}} I(t) dt / \int_0^{t_{lim}} I(t) dt$  becomes  $1-1/e$ , where  $I(t)$  is the intensity at time  $t$  and  $t_{lim}$  is defined as the time when  $I(t_{lim})$  becomes  $0.01I(0)$ . The effective radiative and nonradiative lifetimes ( $\tau_{R,eff}$  and  $\tau_{NR,eff}$ , respectively) are deduced from  $\eta_{int}=(1+\tau_{R,eff}/\tau_{NR,eff})^{-1}$  and  $\tau_{PL(CL),eff}^{-1}=\tau_{R,eff}^{-1}+\tau_{NR,eff}^{-1}$ , where  $\eta_{int}$  is approximated [12] as the spectrally-integrated weakly-excited PL (CL) intensity at given temperature  $T$  over that at around 8~10 K ( $I_{TK}/I_{8K}$ ). Here, the relaxation efficiency toward the radiative NBE states is assumed to be nearly independent of  $T$ .

In order to correlate  $\tau_R$  and  $\tau_{NR}$  with concentrations of cation vacancies ( $V_{III}$ ) and  $V_{III}$ -complexes, PAS measurement [13-15] was carried out using the monoenergetic positron ( $e^+$ ) beam line [12,15,16]. Here,  $S$  parameter [13-15] for the Doppler-broadening spectrum of  $e^+-e^-$  annihila-

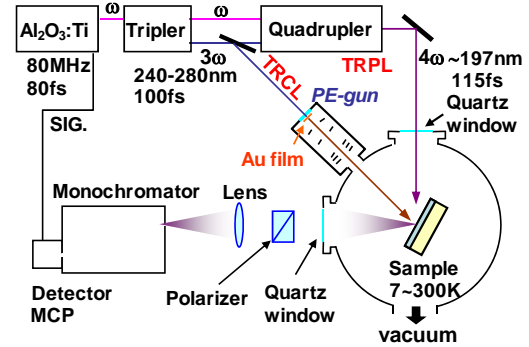


**Figure 1** Schematic drawing of TRPL and TRCL measurement system. (Reproduced from Ref. [7]).

tion  $\gamma$ -rays is used as the measure of concentration or size of negatively charged  $V_{III}$ -defects [13-15]. Details of the measurement and analysis are given in Refs. [12,15,16].

**2.2 Samples** Various quality AlN and Al $_x$ Ga $_{1-x}$ N epilayers [6-9] were grown by low-pressure metalorganic vapor phase epitaxy (MOVPE). In most cases, the reactor pressure was  $2.0 \times 10^4$  Pa.

Approximately 2- $\mu$ m-thick  $c$ -plane AlN films (sample numbers A1~A5) were grown on  $c$ -plane Al $_2$ O $_3$  substrates, and an  $m$ -plane AlN film (A6) was grown on an  $m$ -plane freestanding GaN substrate [17]. The mole flow ratio of NH $_3$  to trimethylaluminium (TMAI) was varied between 32 to 3160. The TD densities having edge components ( $N_E$ ) were  $2 \times 10^8$  cm $^{-2}$  for A1,  $1 \times 10^9$  cm $^{-2}$  for A2 and A6,  $3 \times 10^9$  cm $^{-2}$  for A4 and A5, and  $1 \times 10^{10}$  cm $^{-2}$  for A3 (the values are shown in Fig. 2). The growth temperatures ( $T_g$ ) were 1500°C for A1 and 1350°C for A2 and A3. These samples are classified as high-temperature grown (HTG) samples. Their Si, C, and O concentrations were below the detection limit of secondary-ion-mass spectrometry (below  $5 \times 10^{17}$  cm $^{-3}$ ,  $10^{17}$  cm $^{-3}$ , and  $5 \times 10^{17}$  cm $^{-3}$ , respectively). The low-temperature grown (LTG) AlN samples A4 and A5 were grown at 1200°C, and A6 was grown at 1120°C to prevent GaN substrate from decomposing. Among these, A5 contained high concentration impurities ([Si]≅[C]= $4 \times 10^{19}$  cm $^{-3}$  and [O]= $2 \times 10^{19}$  cm $^{-3}$ ). Those concentrations in A4 and A6 were an order of magnitude lower than A5. All the epilayers exhibited smooth surface morphology with 0.25-nm-high monolayer or 0.50-nm-high bilayer atomic steps.

We also grew approximately 1.3- $\mu$ m-thick (0001) Al $_x$ Ga $_{1-x}$ N epilayers ( $x=0.65, 0.75, 0.89, \text{ and } 0.97$ ) on an 1- $\mu$ m-thick AlN epitaxial template [9], which was grown on a (0001) Al $_2$ O $_3$  substrate. Trimethylgallium (TMGa), TMAI, and NH $_3$  were used as the precursors, and the mole flow ratio of NH $_3$  to sum of TMGa and TMAI was varied between 32 to 3160. The value of  $T_g$  was varied between 1120 and 1200°C. These samples are classified as LTG AlGa $_x$ N. The  $N_E$  values were estimated from the full-width at half-maximum (FWHM) for the {10-12} x-ray rocking curve (1200~1500 arcsec) using the relation given in Ref.

[18] to be  $2\sim 3\times 10^9\text{ cm}^{-2}$ . The TD densities having pure screw components are estimated [18] to be lower than  $2\sim 6\times 10^7\text{ cm}^{-2}$ . They were characterized using the x-ray reciprocal space mapping method to be partially relaxed. The  $x$  values were calculated from the in-plane and out-of-plane lattice parameters and the degree of relaxation using the relation similar to that given in Ref. [19].

### 3 Results and discussion

**3.1 AIN** Room-temperature (RT) and low-temperature (LT) CL spectra for the AIN samples are shown in Fig. 2. As shown, the LT CL spectra for HTG samples are characterized by the predominant sharp excitonic NBE peaks and weak broad emission bands between 4.2 and 2.5 eV. Precisely [6,9], the spectrum of A1 exhibited four bound exciton peaks (6.1040~6.1243 eV), ground state and the first excited state free A-excitonic peaks at  $\text{FX}_A=6.1383$  and  $\text{FX}_{A(n=2)}=6.1768$  eV, respectively, their longitudinal optical (LO) phonon replicas energetically lower than 6.058 eV, and B- and C-excitonic shoulder at  $\text{FX}_{B,C}=6.27$  eV. These energies are higher by 95 meV than the strain-free values due to the in-plane compressive strain [2]. The strongest neutral donor bound exciton peak at 6.1243 eV ( $I_2^1$ ) exhibited the narrowest FWHM being 2.9 meV, indicating reasonable crystal homogeneity. The crystal perfection of A1 is also confirmed by the small  $S$  being 0.458, which is close to the characteristic  $S$  for nearly  $V_{\text{Al}}$ -free ( $[V_{\text{Al}}]<10^{15}$

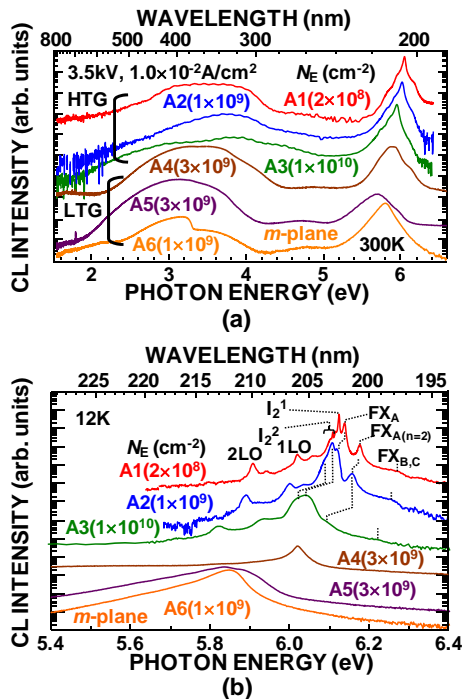


**Figure 2** Steady-state CL spectra of AIN epilayers measured at (a) 300 K and (b) 12 K. The  $N_E$  values are shown in parentheses. FX,  $I_2$ , and LO mean free exciton, neutral donor bound exciton, and LO phonon replica, respectively (Reproduced from Ref. [7]).

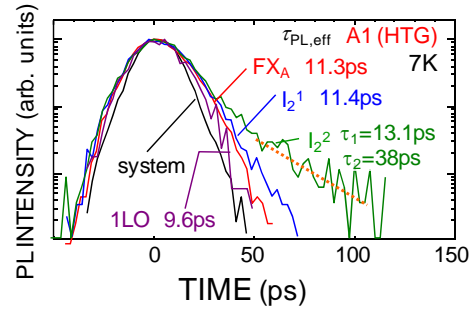


**Figure 3** Energy-resolved TRPL signals for  $\text{FX}_A$ ,  $I_2^1$ ,  $I_2^2$ , and a LO phonon replica of  $\text{FX}_A$  (1LO) peaks in the AIN sample A1 at 7 K. (Reproduced from Ref. [6]).

$\text{cm}^{-3}$ ) AIN ( $S_{\text{free}}$ ) [15].

The CL spectra for LTG ones, in contrast, are characterized by stronger deep-state emission bands and a broad NBE emission band at around 5.7~5.8 eV. For A5 and A6, the NBE CL peak energies were approximately 200 meV lower than  $E_g$  and the FWHM values were as large as 160 meV at 12 K, indicating that the emission originates from certain bound states. Because the deep-state emission bands at 3.1, 3.8, and 4.5 eV have been assigned to originate from point defect complexes involving  $V_{\text{Al}}\text{-O}$  [20-23],  $V_{\text{Al}}\text{-Si}$  [22], and  $V_{\text{Al}}$  [23], respectively, the results suggest a formation of band-tail due to the residual impurities incorporated during LTG. As shown, the spectral feature is not really influenced by  $N_E$ .

Energy-resolved TRPL signals for A1 at 7 K are shown in Fig. 3. The spectra exhibited a single or a double exponential decay shape with very fast lifetime ( $\tau_1$ ). The  $\tau_{\text{PL,eff}}$  value for  $\text{FX}_A$  was as short as 11.3 ps. However, because  $\tau_{\text{PL,eff}}$  for the neutral donor bound excitons  $I_2^1$  and  $I_2^2$  were 11.4~13.1 ps and  $\tau_R$  of free excitons should be shorter than bound excitons,  $\tau_{\text{PL,eff}}$  of  $\text{FX}_A$  may be shorter than 11 ps. It is well-known that measuring lifetime of an LO phonon replica is preferable to determine reliable  $\tau_{\text{PL}}$  in the bulk region. This is because the energies of LO phonon replicas are lower than  $E_g$  and they can come out from the bulk, where any possible effects due to surface recombination can be excluded. As shown in Fig. 3,  $\tau_{\text{PL,eff}}$  of  $\text{FX}_A$ -1LO peak at 6.016 eV was 9.6 ps.

In general,  $\tau_{\text{PL}}$  at LT is governed by  $\tau_R$ , because nonradiative recombination centres (NRCs) are frozen and ideal diffusion lengths of carriers approach nearly zero. Obviously,  $\tau_{\text{PL,eff}}$  of  $\text{FX}_A$  approximately 10 ps is much shorter than general  $\tau_{\text{PL}}$  values reported for GaN (35~220 ps) [24] and ZnO (106 ps) [25]. The  $\tau_{R,\text{eff}}$  value for the NBE emission at LT in III-V and II-VI semiconductors are plotted as a function of  $E_g$  in Fig. 4 [6]. The value of  $\tau_R$  is described [26] as  $\tau_R = 2\pi\epsilon_0 m_0 c^3 / (ne^2 \omega^2 f)$ , where  $f$  is the oscillator strength,  $n$  the refractive index,  $\epsilon_0$  the dielectric constant in vacuum, and  $m_0$  the electron mass in vacuum. As described in Ref. [6],  $\tau_R$  of  $\text{FX}_A$  in AIN is calculated to be 8.4 ns, which is shorter by a factor of 14 than GaN (120 ns).

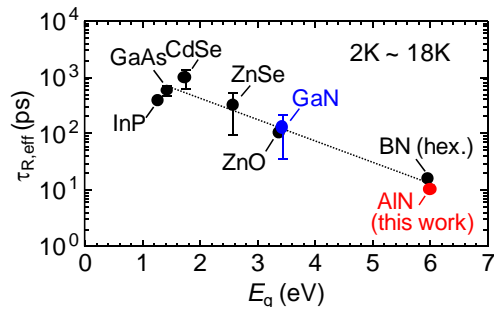


**Figure 4** Low-temperature  $\tau_{R,eff}$  for the NBE emissions in III-V and II-VI compound semiconductors as a function of  $E_g$ . (Reproduced from Ref. [6]).

This trend is consistent with Fig. 4. However, absolute values are 3 orders of magnitude longer than the measured ones. The discrepancy can be partially explained considering the formation of exciton-polaritons [27,28]. Right after excitation, electrons and holes lose their excess energy and momentum within the bands, which usually take sub ps [29]. Subsequently excitons are formed and relax to an exciton-polariton bottleneck, especially at LT. An exciton-polariton is a manifold of an exciton and a light wave that can propagate in a material, and thereby the *polariton lifetime* is the time-of-flight to the surface [28]. This is dependent on energy, in particular around the bottleneck, due to the strong variation of the group velocity. It also depends strongly where the polariton has been created. Then, what one measures could be space-averaged time-of-flight. This is only true if polaritons propagate without collisions. As we have thick samples, elastic collisions may dominate the *polariton lifetime*. Assuming that the *polariton lifetime* near the bottleneck in AlN is close to that calculated for GaN being a few ps [30], the measured lifetime of 10 ps may reflect *whole* processes. Nevertheless, the shortest intrinsic  $\tau_{R,eff}$  at LT in Fig. 4 indicates that the material itself is quite radiative.

Different from HTG samples, TRPL and TRCL signals for LTG AlN (and  $Al_xGa_{1-x}N$ ) samples exhibited a

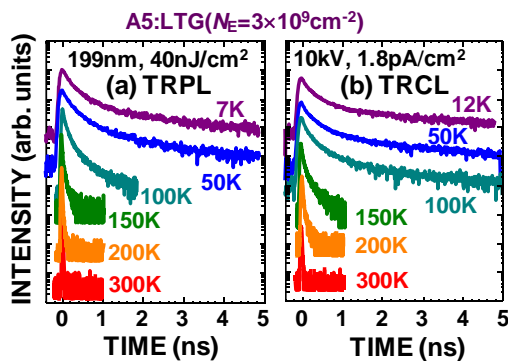


**Figure 5** Temperature variations of (a) TRPL and (b) TRCL signals for the NBE emission of heavily C-, Si-, and O-doped LTG AlN (A5). (Reproduced from Ref. [7]).

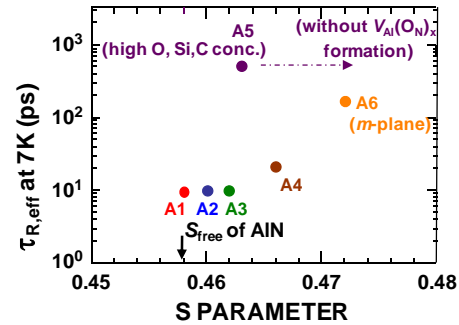


**Figure 6** Low temperature  $\tau_{R,eff}$  for the AlN epilayers as a function of  $S$ . The  $S_{free}$  value for AlN is 0.458. The  $S$  value for A5 is lessened in comparison with other samples due to the formation of  $V_{Al}(O_N)_x$  complexes [15]. (Reproduced from Ref. [7]).

*stretched exponential* decay with slower lifetimes at LT. As shown in Figs. 5(a) and 5(b),  $\tau_{PL(CL),eff}$  value for the NBE emission of A5 at 7 K was as long as 528 ps. This is characteristic of the emission processes in amorphous or defective semiconductors with pronounced tail states [31]. Here we note that in our weak-excitation conditions, TRCL results are quite similar to the TRPL results. The result indicates that TRCL has similar time-resolution as that of TRPL (see the signals at 300 K).

Because donor doping increases  $V_{Al}$  concentration through the Fermi-level effect [32],  $S$  of A4-A6 ( $>0.463$ ) were higher than the HTG series ( $<0.462$ ). Low temperature  $\tau_{R,eff}$  values are plotted as a function of  $S$  in Fig. 6, in which  $S_{free}=0.458$  [15] is marked on the horizontal axis. Considering the fact that  $V_{Al}(O_N)_x$  complexes exhibit smaller characteristic  $S$  than isolated  $V_{Al}$  [15], the result shown in Fig. 6 indicates that  $\tau_{R,eff}$  of excitons bound to high concentration donors (A4) and  $e-h$  pairs bound in band-tail states (A5 and A6) are much longer than the intrinsic  $\tau_{R,eff}$  being of the order of 10 ps. We note that TD itself ( $N_E$ ) has negligible influence on  $\tau_{R,eff}$  (and  $\tau_{NR,eff}$ ).

Temperature dependencies of  $\tau_{R,eff}$  and  $\tau_{NR,eff}$  for A1 and A5 are compared in Fig. 7. For A1,  $\tau_{R,eff}$  monotonically increased according to approximately  $T^{1.5}$  above 130 K, reflecting the increase in kinetic energy of quantum particles in three-dimensional (3D) free space [33]. The value of  $\tau_{R,eff}$  reached 183 ps at 300 K. However, this is still the shortest among the semiconductors shown in Fig. 4. Due to the thermal activation of NRCs,  $\tau_{NR,eff}$  decreased with  $T$ . On the contrary,  $\tau_{R,eff}$  for the NBE emission of A5 first decreased with  $T$  up to 200 K. The result may reflect a recovery in  $f$  of  $e-h$  pairs, as follows: they are spatially-separated in the conduction band minima (CBM) and valence band maxima (VBM) at low-temperature, as schematically shown in Fig. 7(b), where CBM and VBM are formed due to charged impurities and counter-charged point defects. As  $T$  increases, the carriers may be released to 3D space to gain the wavefunction overlap. Above 230 K,  $\tau_{R,eff}$  increases with  $T^{1.5}$ . The decrease in  $\tau_{NR,eff}$  with  $T$  in A5 is

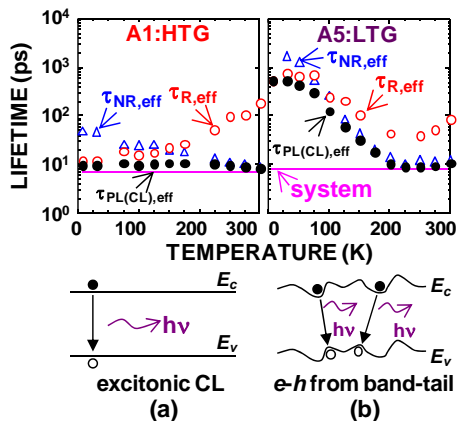


**Figure 7** Temperature dependencies of measured  $\tau_{\text{PL(CL),eff}}$  and calculated  $\tau_{\text{R,eff}}$  and  $\tau_{\text{NR,eff}}$  for the AlN epilayers (a) HTG A1 and (b) LTG A5. (Reproduced from Ref. [7]).

much remarkable than A1, reflecting enhanced carrier capture by NRCs due to the carrier release from the tail-states. Because the change in  $\tau_{\text{NR,eff}}$  at 300 K was only from 10 ps to 7 ps with the increase in  $S$  and both are close to the time resolution, assertive conclusion cannot be drawn on the relation between  $\tau_{\text{NR,eff}}$  and  $V_{\text{Al}}$  concentration. However, similar to the case for GaN [12] and ZnO [25],  $V_{\text{Al}}$ -complexes may act as a severe NRC in AlN.

### 3.2 High AlN mole fraction $\text{Al}_x\text{Ga}_{1-x}\text{N}$ alloys

Steady-state PL or CL spectra at LT for the  $\text{Al}_x\text{Ga}_{1-x}\text{N}$  epilayers are shown in Fig.8. Their spectra exhibited a spectrally broad but reasonably intense NBE peak. Similar to the results reported previously [16,34,35], their peak energies are lower by approximately 200 meV than  $E_g$ . As shown, the luminescence intensities for the deep-state emission bands below 4.4 eV are two or three orders of magnitude weaker than the NBE peak. However, because these films are LTG, band-tail formation and compositional inhomogeneity are hard to avoid.

Compositional variations in the FWHM value for the NBE emission at 8 K,  $S$  parameter,  $\tau_{\text{R,eff}}$ (8 K),  $\tau_{\text{R,eff}}$ (300 K), and  $\tau_{\text{NR,eff}}$ (300 K) for the  $\text{Al}_x\text{Ga}_{1-x}\text{N}$  epilayers are shown in

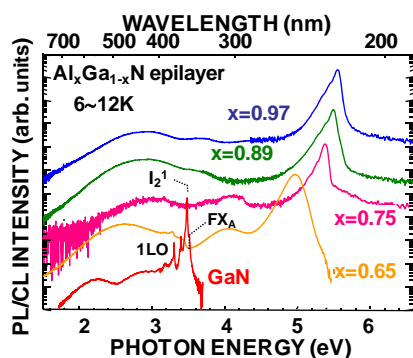


**Figure 8** Steady-state PL and CL spectra at 6~12K for the  $\text{Al}_x\text{Ga}_{1-x}\text{N}$  alloy epilayers grown by MOVPE. (Reproduced from Ref. [8]).

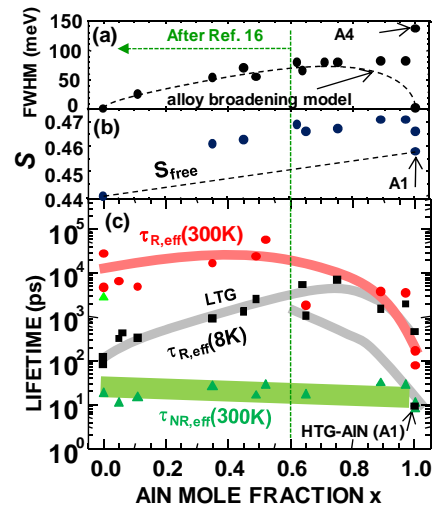


**Figure 9** (a) FWHM value for the NBE emission at 8 K, (b)  $S$  parameter, and (c)  $\tau_{\text{R,eff}}$  at 8 K,  $\tau_{\text{R,eff}}$  at 300 K, and  $\tau_{\text{NR,eff}}$  at 300 K for the NBE emission of  $\text{Al}_x\text{Ga}_{1-x}\text{N}$  epilayers. The samples of  $x < 0.64$  were grown at 1150 °C [16]. (Reproduced from Ref. [8]).

Fig. 9. The samples of  $x < 0.64$  were grown at 1150 °C on a (0001)  $\text{Al}_2\text{O}_3$  substrate [16]. The dashed curve in Fig. 9(a) shows the calculated FWHM value [16] for the NBE emission of statistically homogeneous  $\text{Al}_x\text{Ga}_{1-x}\text{N}$  according to alloy-broadening model [36]. The dashed line in Fig. 9(b) connects the  $S_{\text{free}}$  values of GaN [8,12] and AlN [7,8,15], which represents  $S_{\text{free}}$  of  $\text{Al}_x\text{Ga}_{1-x}\text{N}$  alloys. From the figure, following tendency can be extracted. Because  $T_g$  was insufficient, FWHM values for the NBE emission are larger than the ideal values. In addition,  $S$  of all the epilayers are larger than  $S_{\text{free}}$ , meaning that present samples contain high concentration  $V_{\text{III}}$ -defects. As the formation energy of  $V_{\text{Al}}$  in AlN is far lower than that of Ga vacancies in GaN and even negative for  $n$ -type sample [32], major  $V_{\text{III}}$ -defect in  $\text{Al}_x\text{Ga}_{1-x}\text{N}$  is assigned to  $V_{\text{Al}}$ . The simultaneous increase in  $\tau_{\text{R,eff}}$ (8 K) and  $S$  for LTG  $\text{Al}_x\text{Ga}_{1-x}\text{N}$ , therefore, means that certain point-defect complexes involving  $V_{\text{Al}}$  produce the band-tail to elongate  $\tau_{\text{R,eff}}$ (8 K), as is the case with AlN [7].

Conversely, however,  $\tau_{\text{R,eff}}$ (300 K) decreases with increasing  $x$ , at least for  $x > 0.4$ . This is consistent with the fact that  $f$  for 3D  $e$ - $h$  pairs (excitons) in AlN is approximately 4 to 10 times that of GaN [6-8,37]. As a matter of fact,  $\tau_{\text{R,eff}}$  values for HTG AlN are as short as 10 ps at 8 K and 180 ps at 300 K [7]. Therefore, although  $\tau_{\text{R,eff}}$  values at 8 K are longer than the expected ones, room temperature  $\tau_{\text{R,eff}}$  being in the order of a few ns for the  $\text{Al}_x\text{Ga}_{1-x}\text{N}$  alloys of high  $x$  are reasonably short, being comparable to or even shorter than that of GaN and InGaN films [12].

**4 Conclusion** Extremely radiative nature of AlN is revealed from the short  $\tau_{\text{R,eff}}$  for the excitonic polariton emission (10 ps at 7 K and 180 ps at RT). However, the  $\tau_{\text{R,eff}}$  value increases with the increase in impurity and  $V_{\text{Al}}$

concentrations up to 530 ps at 7 K, irrespective of  $N_E$ . Continuous decrease in  $\tau_R$  with temperature rise up to 200 K for LTG AlN may reflect the dominance of the emission from band-tail states formed due to impurities and point defects. For LTG high- $x$   $\text{Al}_x\text{Ga}_{1-x}\text{N}$  epilayers,  $\tau_R$  is elongated due to the contribution of band-tail states. However,  $\tau_R$  shows little change with temperature rise, and the value is still a few ns at 300 K. The results indicate that high- $x$   $\text{Al}_x\text{Ga}_{1-x}\text{N}$  also has an excellent radiative nature. Because point defects and impurities, rather than TDs, limit  $\tau_R$  (and  $\tau_{NR}$ ), HT growth and appropriate defect management are necessary in extracting their radiative performance.

**Acknowledgements** The authors thank Prof. T. Sota of Waseda Univ., Prof. C. Weisbuch of Univ. California Santa Barbara, Prof. B. Gil of Univ. Montpellier II, and Dr. M. Tanaka for fruitful discussions. This work was supported in part by NEDO programs under METI, Grant-in-Aids for Scientific Research Nos. 23656206 and 18069001 under MEXT, Japan, and AFOSR/AOARD Grant Nos. FA2386-11-1-4013 and FA2386-11-1-4108 monitored by Dr. G. Jessen.

## References

- [1] B. Gil, *Phys. Rev. B* **81**, 205201 (2010).
- [2] H. Ikeda, T. Okamura, K. Matsukawa, T. Sota, M. Sugawara, T. Hoshi, P. Cantu, R. Sharma, J. F. Kaeding, S. Keller, U. K. Mishra, K. Kosaka, K. Asai, S. Sumiya, T. Shibata, M. Tanaka, J. S. Speck, S. P. DenBaars, S. Nakamura, T. Koyama, T. Onuma, and S. F. Chichibu, *J. Appl. Phys.* **102**, 123707 (2007); erratum in *J. Appl. Phys.* **103**, 089901 (2008).
- [3] Y. Taniyasu, M. Kasu, and T. Makimoto, *Nature* **441**, 325 (2006).
- [4] Quantum efficiencies of state-of-the-art UV LEDs are described in C. Pernot, M. Kim, S. Fukahori, T. Inazu, T. Fujita, Y. Nagasawa, A. Hirano, M. Ippommatsu, M. Iwaya, S. Kamiyama, I. Akasaki, and H. Amano, *Appl. Phys. Express* **3**, 061004 (2010) and references cited therein.
- [5] K. B. Nam, J. Li, M. L. Nakarmi, J. Y. Lin, and H. X. Jiang, *Appl. Phys. Lett.* **82**, 1694 (2003).
- [6] T. Onuma, K. Hazu, A. Uedono, T. Sota, and S. F. Chichibu, *Appl. Phys. Lett.* **96**, 061906 (2010).
- [7] S. F. Chichibu, T. Onuma, K. Hazu, and A. Uedono, *Appl. Phys. Lett.* **97**, 201904 (2010).
- [8] S. F. Chichibu, K. Hazu, T. Onuma, and A. Uedono, *Appl. Phys. Lett.* **99**, 051902 (2011).
- [9] T. Onuma, T. Shibata, K. Kosaka, K. Asai, S. Sumiya, M. Tanaka, T. Sota, A. Uedono, and S. F. Chichibu, *J. Appl. Phys.* **105**, 023529 (2009).
- [10] T. Onuma, Y. Kagamitani, K. Hazu, T. Ishiguro, T. Fukuda, and S. F. Chichibu, *Rev. Sci. Instrum.* **83**, 043905 (2012).
- [11] M. Merano, S. Collin, P. Renucci, M. Gatri, S. Sonderegger, A. Crottini, J. D. Ganiere, and B. Deveaud, *Rev. Sci. Instrum.* **76**, 085108 (2005).
- [12] S. F. Chichibu, A. Uedono, T. Onuma, B. A. Haskell, A. Chakraborty, T. Koyama, P. T. Fini, S. Keller, S. P. DenBaars, J. S. Speck, U. K. Mishra, S. Nakamura, S. Yamaguchi, S. Kamiyama, H. Amano, I. Akasaki, J. Han, and T. Sota, *Nature Mater.* **5**, 810 (2006); *Philos. Mag.* **87**, 2019 (2007).
- [13] R. Krause-Rehberg and H. S. Leipner, *Positron Annihilation in Semiconductors*, Solid-State Sciences (Springer, Berlin, 1999) Vol. 127.
- [14] P. G. Coleman, *Positron Beams and Their Application*, (World Scientific, Singapore, 2000).
- [15] A. Uedono, S. Ishibashi, S. Keller, C. Moe, P. Cantu, T. M. Katona, D. S. Kamber, Y. Wu, E. Letts, S. A. Newman, S. Nakamura, J. S. Speck, U. K. Mishra, S. P. DenBaars, T. Onuma, and S. F. Chichibu, *J. Appl. Phys.* **105**, 054501 (2009).
- [16] T. Onuma, S. F. Chichibu, A. Uedono, T. Sota, P. Cantu, T. M. Katona, J. F. Keady, S. Keller, U. K. Mishra, S. Nakamura, and S. P. DenBaars, *J. Appl. Phys.* **95**, 2495 (2004).
- [17] K. Fujito, K. Kiyomi, T. Mochizuki, H. Oota, H. Namita, S. Nagao, and I. Fujimura, *Phys. Status Solidi A* **205**, 1056 (2008).
- [18] C. G. Dunn and E. F. Koch, *Acta Metall.* **5**, 548 (1957).
- [19] K. Hazu, M. Kagaya, T. Hoshi, T. Onuma, and S. F. Chichibu, *J. Vac. Sci. Technol. B* **29**, 021208 (2011).
- [20] G. A. Slack, L. J. Schowalter, D. Morelli, and J. A. Freitas, Jr., *J. Cryst. Growth* **246**, 287 (2002).
- [21] K. B. Nam, M. L. Nakarmi, J. Y. Lin, and H. X. Jiang, *Appl. Phys. Lett.* **86**, 222108 (2005).
- [22] A. Dadgar, A. Krost, J. Christen, B. Bastek, F. Bertram, A. Krtischil, T. Hempel, J. Blasing, U. Haboeck, and A. Hoffmann, *J. Cryst. Growth* **297**, 306 (2006).
- [23] T. Koyama, M. Sugawara, T. Hoshi, A. Uedono, J. F. Kaeding, R. Sharma, S. Nakamura, and S. F. Chichibu, *Appl. Phys. Lett.* **90**, 241914 (2007).
- [24] For example, see G. Pozina, J. P. Bergman, T. Paskova, and B. Monemar, *Appl. Phys. Lett.* **75**, 4124 (1999).
- [25] S. F. Chichibu, T. Onuma, M. Kubota, A. Uedono, T. Sota, A. Tsukazaki, A. Ohtomo, and M. Kawasaki, *J. Appl. Phys.* **99**, 093505 (2006).
- [26] G. W. 't Hooft, W. A. J. A. van der Poel, L. W. Molenkamp, and C. T. Foxon, *Phys. Rev. B* **35**, 8281 (1987).
- [27] H. Sumi, *J. Phys. Soc. Japan* **41**, 526 (1976).
- [28] C. Weisbuch, H. Benisty, and R. Houdre, *J. Luminescence* **85**, 271 (2000).
- [29] J. Shah, *Ultrafast spectroscopy of semiconductors and semiconductor nanostructures*, (Springer, Berlin, 1996).
- [30] K. Torii, T. Deguchi, T. Sota, K. Suzuki, S. Chichibu, and S. Nakamura, *Phys. Rev. B* **60**, 4723 (1999).
- [31] R. Kohlrausch, *Ann. Phys.* **12**, 393 (1847).
- [32] C. Stampfl and C. G. Van de Walle, *Appl. Phys. Lett.* **72**, 459 (1998).
- [33] J. Feldmann, G. Peter, E. O. Göbel, P. Dawson, K. Moore, C. Foxon, and R. J. Elliot, *Phys. Rev. Lett.* **59**, 2337 (1987).
- [34] N. Teofilov, K. Thonke, R. Sauer, L. Kirste, D. G. Ebling, K. W. Benz, *Diamond and Related Mater.* **11**, 892 (2002).
- [35] H. Murotani, Y. Yamada, H. Miyake, and K. Hiramatsu, *Appl. Phys. Lett.* **98**, 021910 (2011).
- [36] E. F. Schubert, E. O. Göbel, Y. Horikoshi, K. H. Ploog, and H. J. Queisser, *Phys. Rev. B* **30**, 813 (1984).
- [37] H. Murotani, T. Kuronaka, Y. Yamada, T. Taguchi, N. Okada, and H. Amano, *J. Appl. Phys.* **105**, 083533 (2009).

## Spatio-Time-Resolved Cathodoluminescence Studies on Freestanding GaN Substrates Grown by Hydride Vapor Phase Epitaxy

S. F. Chichibu<sup>a</sup>, Y. Ishikawa<sup>a</sup>, M. Tashiro<sup>a</sup>, K. Hazu<sup>a</sup>, K. Furusawa<sup>a</sup>, H. Namita<sup>b</sup>, S. Nagao<sup>b</sup>, K. Fujito<sup>b</sup>, and A. Uedono<sup>c</sup>

<sup>a</sup> Institute of Multidisciplinary Research for Advanced Materials, Tohoku University, 2-1-1 Katahira, Aoba, Sendai 980-8577, Japan

<sup>b</sup> Gallium Nitride Department, Mitsubishi Chemical Corporation, 1000 Higashi-Mamiana, Ushiku 300-1295, Japan

<sup>c</sup> Division of Applied Physics, University of Tsukuba, 1-1-1 Tennodai, Tsukuba, Ibaraki 305-8573, Japan

A spatio-time-resolved cathodoluminescence (STRCL) system was constructed by replacing the electron beam (*e*-beam) gun of a conventional scanning electron microscope by the in-house manufactured pulsed *e*-beam gun, which is excited using femtosecond laser pulses. By using this system, STRCL measurements were carried out on low threading dislocation density freestanding GaN substrates grown by hydride vapor phase epitaxy. High-resolution cathodoluminescence imaging allows for visualization of nonradiative recombination channels in the vicinity of accidentally formed domain boundaries. Local cathodoluminescence lifetimes ( $\tau_{\text{CL}}$ ) for the near-band-edge (NBE) emission are shown to be sensitively position dependent. A linear relation between the equivalent internal quantum efficiency ( $\eta_{\text{int}}^{\text{eq}}$ ) and  $\tau_{\text{CL}}$  for the NBE emission was observed at room temperature under a weak excitation condition, and spatially resolved excitation led to the observation of the highest  $\eta_{\text{int}}^{\text{eq}}$  of 20 % with  $\tau_{\text{CL}}$  of 3.3 ns.

### Introduction

As a solution to concerns about energy crisis, exploitation of high-efficiency power-switching devices using AlGaIn/GaN heterostructure-field-effect-transistors and solid-state-lighting using InGaIn quantum well light-emitting-diodes (LEDs) is one of the significant ways for drastically decreasing total energy consumption (1). Whilst InGaIn LEDs fabricated on defective *GaN templates* grown on (0001) sapphire substrates, which have high density threading dislocations (TDs) typically  $10^8 \sim 10^9 \text{ cm}^{-2}$ , are commercially available thanks to the defect-insensitive emission probability of InGaIn alloys (2-7), it becomes evident that high-purity, large-area, free-standing GaN (FS-GaN) wafers with low threading dislocation density (TDD) are necessary not only for achieving ultimate performance and/or excellent reliabilities of optical devices but also for realizing AlGaIn/GaN power-switching transistors. Especially, suppression of the *efficiency-droop* phenomenon in InGaIn LEDs is predicted for the devices grown on off-polar plane, heat-conducting FS-GaN substrates.

For fabricating such substrates, hydride vapor phase epitaxy (HVPE) is one of the most commonly-accepted techniques (8) despite cumulative bowing of the crystal plane that arises from the mismatch of the thermal expansion coefficients between GaN and the substrate. Indeed, both *c*-plane and off-polar plane FS-GaN wafers with significantly reduced TDD ( $<10^7 \text{ cm}^{-2}$ ) and low basal-plane stacking fault (BSF) density ( $<10^3 \text{ cm}^{-1}$ ) are distributed (8,9). From scientific point of view, fundamental influences by point defects on the electronic and optical properties can be studied using such low structural defect density, high-purity bulk crystals. For instance, equivalent internal quantum efficiency ( $\eta_{\text{int}}^{\text{eq}}$ ) for the near-band-edge (NBE) emission is determined by the balance between the radiative and nonradiative recombination rates;  $\eta_{\text{int}}^{\text{eq}} = (1 + \tau_{\text{R}}/\tau_{\text{NR}})^{-1}$ , where  $\tau_{\text{R}}$  and  $\tau_{\text{NR}}$  are the radiative and nonradiative lifetimes, respectively. As  $\tau_{\text{NR}}$  for the NBE emission of GaN has been correlated with the gross concentration of point defects and complexes (10,11) rather than TDD, understanding local carrier (exciton) recombination dynamics within low structural defect density areas of a GaN substrate is of paramount importance.

Because state-of-the-art low TDD FS-GaN substrates are of high quality, the influence of a TD on the local luminescence spectrum and lifetime can be studied using a spectroscopy technique of sufficient high spatial resolution. In order to probe local carrier dynamics in wide bandgap ( $E_g$ ) semiconductors, scanning near-field optical microscopy (SNOM) with a short-pulsed laser is widely used. On the other hand, the use of a scanning electron microscopy (SEM) equipped with a femtosecond electron beam (*e*-beam) gun (12-18), namely spatio-time-resolved cathodoluminescence (STRCL) technique (13,14,16,18), makes it possible to measure local time-resolved cathodoluminescence (TRCL) signals at the positions defined precisely by the secondary electron (SE) image. This becomes attractive when characterizing very wide  $E_g$  materials such as AlN and  $\text{Al}_x\text{Ga}_{1-x}\text{N}$  alloys of high AlN mole fraction  $x$ . Indeed, STRCL takes full advantage of such a pulsed *e*-beam, which enables high spatial resolution beyond the diffraction limit of light owing to the focused electronic excitation and thus makes it possible to interrogate local carrier/exciton dynamics. Unique opportunities offered by the STRCL demonstrated so far includes the investigations of the exciton dynamics around BSFs in an *a*-plane GaN (14) and the slight local variations of In incorporation in the  $\text{In}_{0.05}\text{Ga}_{0.95}\text{N}$  epilayer (16) grown on an *m*-plane FS-GaN.

In this transaction, the correlation between the local cathodoluminescence (CL) intensities and lifetimes for the NBE emission of low TDD FS-GaN substrates grown by HVPE (8) is demonstrated using the STRCL technique. In the vicinity of an accidentally-formed trapezoidal dimple surrounded by domain boundaries (DBs), the spatial variations of  $\tau_{\text{CL}}$  and carrier/exciton diffusion length ( $L_d$ ) are clearly visualized.

## Experimental

### Samples

The samples investigated herein were approximately 500- $\mu\text{m}$ -thick *c*-plane FS-GaN substrates named A1 and A2, which were grown using a vertical-flow HVPE apparatus (8,9). Appropriate amount of gaseous HCl was flowed on heated Ga, and  $\text{NH}_3$  was supplied from a separate gas line. The growth temperature and pressure were 1050 °C and atmospheric pressure, respectively. The electron concentrations were  $3 \times 10^{18}$  and  $2 \times 10^{17} \text{ cm}^{-3}$  for samples A1 and A2, respectively. The TDDs were estimated from the

full-width at half-maximum (FWHM) values of the x-ray rocking curves (XRCs) using the relation given in Ref. (19). Those containing edge components ( $N_E$ ) were estimated to be  $6.6 \times 10^6$  and  $6.3 \times 10^6$   $\text{cm}^{-2}$  for A1 and A2, respectively. The  $S$  parameters obtained from the positron annihilation measurement, which reflect the concentration and/or size of Ga vacancies ( $V_{\text{Ga}}$ ) and  $V_{\text{Ga}}$ -complexes, of the present samples were close to (11) characteristic  $S$  for vacancy-free GaN ( $S_{\text{free}}$ ) being 0.442, which was calculated using the first principles calculations (20). We note that  $V_{\text{Ga}}$ -defect concentration in the sample exhibiting  $S_{\text{free}}$  is lower than the detection limit for GaN ( $\cong 10^{15}$   $\text{cm}^{-3}$ ) (20), which corresponds to the concentration that positron trapping probability reaches zero. Details of the growth (8,9) and fundamental optical properties (11) have been given in literatures.

Prior to STRCL measurement, macroarea steady-state photoluminescence (PL) and time-resolved photoluminescence (TRPL) measurements were carried out using the 325 nm line of a cw He-Cd laser with an excitation intensity of  $20$   $\text{W}/\text{cm}^2$  and a frequency-tripled mode-locked  $\text{Al}_2\text{O}_3:\text{Ti}$  laser operating at a wavelength of 267 nm ( $200$   $\text{nJ}/\text{cm}^2$ ), respectively. Note that for both cases, weak excitation conditions were maintained, meaning that the excited carrier concentration was lower than that of the residual carriers.

### Spatio-Time-Resolved Cathodoluminescence Measurement

Schematic diagram of our STRCL equipment is shown in Fig. 1. The system (18) consists of an SEM equipped with an in-house photoelectron gun (PE-gun) (15,17), which was driven by a frequency-tripled mode-locked  $\text{Al}_2\text{O}_3:\text{Ti}$  laser pulses. The beam was focused using a fused silica lens ( $f=300$  mm) with a spot diameter of  $50$   $\mu\text{m}$  to a rear-side of a photocathode. The average power of  $80$  mW was used at a repetition rate of  $80$  MHz, corresponding to laser fluence of  $32$   $\mu\text{J}/\text{cm}^2$ . This value was limited by the onset of optical damage of the photocathode. The output  $e$ -beam was launched to the SEM by focusing it to its filament position. The probe current was calibrated using a Faraday cup placed just above the temperature-controlled stage, and was typically  $20$  nA at an

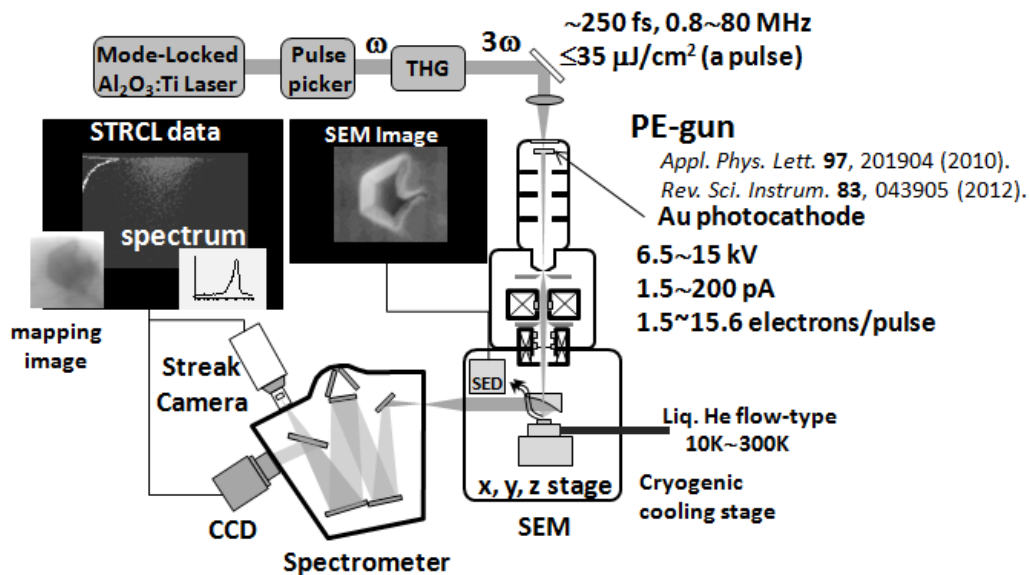


Figure 1. Schematic diagram of the STRCL measurement system. The wavelength and repetition rate of the frequency-tripled ( $3\omega$ ) femtosecond  $\text{Al}_2\text{O}_3:\text{Ti}$  laser are adjusted according to the purpose of the measurement.

acceleration voltage ( $V_{acc}$ ) of 10 kV. Although this is smaller than what can be achieved with a conventional W filament, reasonable quality of SEM images can be obtained. The luminescence from a sample was collected using an off-axis parabolic mirror ( $R=12$  mm) placed above the sample and then analyzed using a grating spectrometer equipped with an electronically-cooled charged-coupled device and a streak camera with a temporal resolution of approximately 10 ps.

## Results and Discussion

Figure 2(a) shows a representative macroarea PL spectrum of A1 at 293 K. The sample exhibited a predominant NBE peak at 3.373 eV with the FWHM value of 73 meV and its LO phonon replica (a shoulder peak) at around 3.28 eV. The peak intensity of the broad emission band at around 2.2 eV (so-called yellow luminescence band) was more than three orders of magnitude lower than that of the NBE emission. The sample A2 showed an essentially the same spectrum, indicating that both samples are of excellent quality.

Figure 2(b) shows room temperature TRPL decay signals for the NBE emission in A1, measured at three different positions. It is found that characteristic lifetimes of the fast decay components ( $\tau_1$ ) were strongly position dependent, varying from 0.47 to 1.24 ns, although the overall PL spectra were almost unchanged (data not shown). The result implies that room temperature  $\tau_{NR}$  varies depending on the positions.

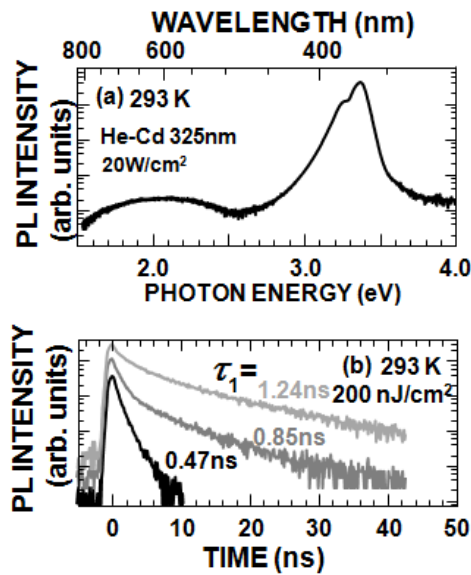


Figure 2 (a) A macroarea steady-state PL spectrum at 293 K and (b) macroarea TRPL decay signals taken at 293 K for the NBE emission of the FS-GaN substrate grown by HVPE (A1). The TRPL signals were taken from three different positions, and vertical offsets are given for better looking.

In order to visualize spatial variations of the luminescence intensity and to evaluate local  $\tau_{NR}$  for the NBE emission, STRCL measurement was conducted near the region surrounded by the DBs in A1. We note that such DBs are occasionally formed by some growth perturbations. Figures 3(a), 3(b), and 3(c), respectively, illustrate SEM image and CL intensity images recorded for the NBE emission at 293 K and 20 K. These CL images

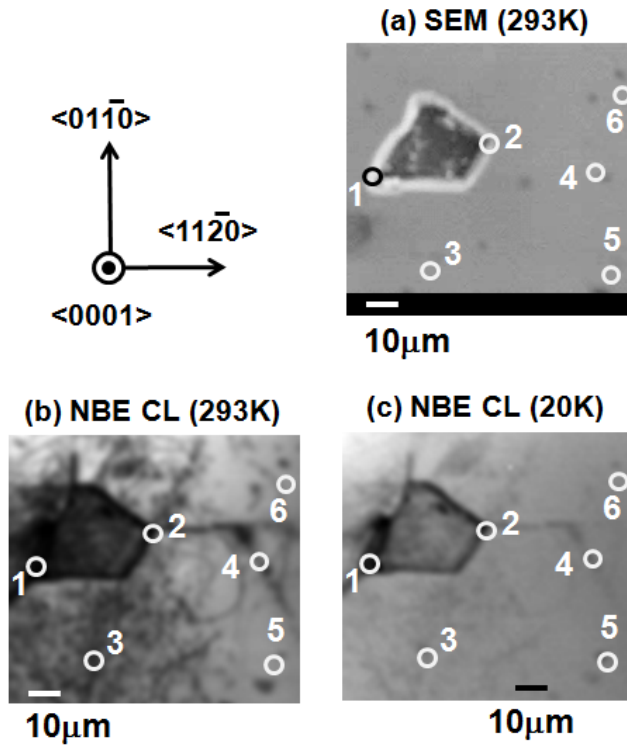


Figure 3 (a) A macroarea steady-state PL spectrum at 293 K and (b) macroarea TRPL decay signals taken at 293 K for the NBE emission of the FS-GaN substrate grown by HVPE (A1). The TRPL signals were taken from three different positions, and vertical offsets are given for better looking.

were taken with a probe current of 100 pA and a dwell time of 200 ms, corresponding to 30 minutes per image. The SEM image showed a trapezoidal dimple surrounded by the DBs. Also, several dark spots were found although their contrasts were rather faint. These spots were also observed as the dark spots in the CL image at 293 K, as shown in Fig. 3(b). The CL image at 293 K showed complex structures since its contrast reflects spatial distribution of nonradiative recombination centers (NRCs) while its spatial resolution is limited by  $L_d=(D\cdot\tau)^{1/2}$  of minority carriers (21), where  $D$  and  $\tau$  are their diffusivity and lifetime, respectively. The sharpness of the CL image taken at 20 K was greatly improved because  $D$  approaches to zero towards 0 K according to Einstein's relation  $D=k_B T\mu/q$ , where  $k_B$  is the Boltzmann constant,  $T$  the temperature,  $q$  the electric charge, and  $\mu$  the mobility. Furthermore, since the NRCs are essentially frozen out at low temperatures, contributions from pure NRCs are excluded in Fig. 3(c). Therefore, the dark areas and lines that remain in Fig. 3(c) are possibly due to the absence of the material itself or the presence of extremely strong NRCs. In both Figs. 3(b) and 3(c), it can be seen that some straight line structures run from the corners of the trapezoid parallel to  $m$ -planes. This implies that the tensile stress accumulated around the DBs is relaxed by introducing cracks. Since there are no corresponding structures in the SEM image, it is likely that these cracks run under the surface, and which can specifically be detected in the CL images due to the finite implantation depth of the  $e$ -beam and the longitudinal diffusion of the minority carriers.

The virtue of STRCL is that it is readily accessible to the local recombination dynamics for a particular emission peak. Local time-integrated cathodoluminescence (TICL) and TRCL decay signals for the NBE emission of A1 measured at room

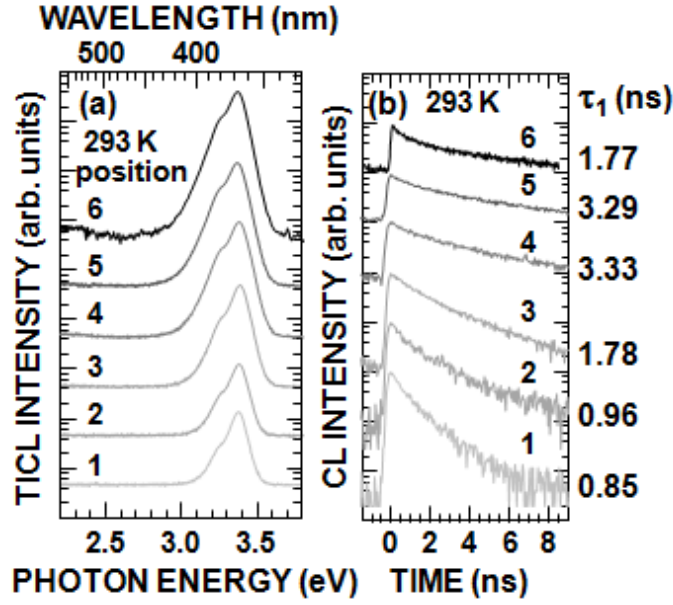


Figure 4 Position dependent TICL spectra (a) and TRCL decay signals (b) for the NBE emission of FS-GaN sample A1 measured at 293 K. The number corresponds to the position encircled in Fig. 3.

temperature at the positions encircled in Fig. 3 are shown in Figs. 4(a) and 4(b), respectively. In this instance, the probe current was decreased to 25 pA, which amounts to 2 electrons per pulse, in order to prevent any degradation in temporal resolution (17). The resultant number of excited electron-hole pairs in GaN are deduced to be less than 2000 from the empirical relation given in Ref. (22). We note that this excitation density gives the  $\tau_1$  value for the TRPL decay constant of a GaN template when excited with the laser fluence of  $2 \mu\text{J}/\text{cm}^2$  (17). This value is an order of magnitude higher than that used for the TRPL measurement. However, weak excitation conditions are still maintained. The nominal NBE peak energy was approximately 3.38 eV while the FWHM values were 90 meV, both of which are in reasonable agreement with Fig. 2(a). In these spectra, we found subtle redshifts of the NBE emission peak inside and on the peripheries of the trapezoid. This can be attributed to the local strain or increased residual electron concentration. We fit the decay curves by a double exponential function to extract  $\tau_1$ , and found that  $\tau_1$  significantly varied depending on the positions. The decrease of  $\tau_1$  near the visual defects in the CL image at 293 K [see Fig. 3(b)] can be understood as enhanced recombination at NRCs because  $\tau_1$  at room temperature is generally dominated by  $\tau_{\text{NR}}$ . By contrast, local  $\tau_1$  values measured at 10 K were almost independent of the positions being 180 ps. This is reasonable since  $\tau_{\text{R}}$  dominates  $\tau_{\text{CL}}$  at low temperature.

We also evaluated the local  $\eta_{\text{int}}^{\text{eq}}$  for the NBE emission by simply taking the ratio of the integrated spectral intensities at 293 K to that at 20 K. The results for A1 and A2 are summarized as a function of  $\tau_1$  in Fig. 5. The best data for the macroarea PL measurement on similar HVPE FS-GaN (11) and typical values observed for GaN templates are also plotted for reference. As shown,  $\eta_{\text{int}}^{\text{eq}}$  linearly increases with the increase in  $\tau_1$  according to  $\eta_{\text{int}}^{\text{eq}} = (1 + \tau_{\text{R}}/\tau_{\text{NR}})^{-1}$ , where we assume that  $\tau_{\text{R}}$  is an intrinsic value to a particular material (23) and that  $\tau_{\text{CL}}$  is generally dominated by  $\tau_{\text{NR}}$  at room temperature under the relation  $\tau_{\text{CL}}^{-1} = \tau_{\text{R}}^{-1} + \tau_{\text{NR}}^{-1}$ . Although the overall trend of higher  $\eta_{\text{int}}^{\text{eq}}$  in the local measurement may indicate somewhat higher excitation density used, the

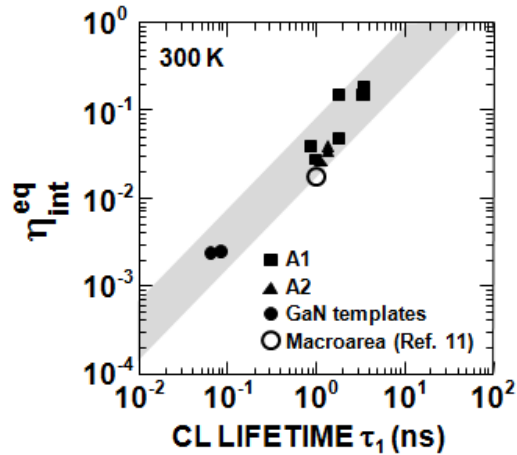


Figure 5 The values of  $\eta_{int}^{eq}$  for the NBE emission peak of FS-GaN samples at room temperature as a function of the fast decay constant ( $\tau_1$ ) obtained from the STRCL measurement. The results for the macroarea measurement for both the HVPE FS-GaN (sample C0 in Ref. (11)) that exhibited the longest positron diffusion length ( $L_+ = 116$  nm) and GaN templates are also included for reference.

spatially focused excitation in STRCL can selectively probe highly luminescent regions that are less affected by NRCs. As a result, a record high  $\eta_{int}^{eq}$  of up to 20% was obtained for position 4 in 3, where  $\tau_1$  was as long as 3.33 ns.

## Conclusions

Local carrier recombination dynamics in the low TDD FS-GaN substrates grown by HVPE were studied by STRCL measurement. In addition to the visualization of defect networks originating from the DBs in the CL intensity images, the spatially resolved TICL and TRCL measurements revealed a linear correlation between  $\eta_{int}^{eq}$  and  $\tau_{CL}$  at room temperature. The spatially focused excitation led us to observe the highest  $\eta_{int}^{eq}$  of 20% and the longest  $\tau_{CL}$  of 3.33 ns at 293 K. We believe that our results demonstrate the potential of FS-GaN grown by HVPE and serves as a benchmark for future development.

## Acknowledgments

This work was supported in part by NEDO programs by METI, Grant-in-Aids for Scientific Research (Nos. 23656206 and 24760250) from MEXT, Japan, and AOARD/AFOSR monitored by G. Jessen.

## References

1. A. Nagahira, D. Probert, T. Fukuda, S. F. Chichibu, Y. Kagamitani, and A. Abe, Proceedings of the R&D Management Conference (2010), Roadmapping Session, Vol. 1, Article No.2, pp.9-23.
2. S. F. Chichibu, T. Azuhata, T. Sota, and S. Nakamura, *Appl. Phys. Lett.* **69**, 4188 (1996).

3. S. F. Chichibu, A. C. Abare, M. P. Mack, M. S. Minsky, T. Deguchi, D. Cohen, P. Kozodoy, S. B. Fleischer, S. Keller, J. S. Speck, J. E. Bowers, E. Hu, U. K. Mishra, L. A. Coldren, S. P. DenBaars, K. Wada, T. Sota, and S. Nakamura, *Mater. Sci. Eng. B* **59**, 298 (1999).
4. Y. Narukawa, Y. Kawakami, S. Fujita, S. Fujita, and S. Nakamura, *Phys. Rev. B* **55**, R1938 (1997).
5. L. Bellaiche, T. Mattila, L. -W. Wang, S. -H. Wei, and A. Zunger, *Appl. Phys. Lett.* **74**, 1842 (1999).
6. P. R. C. Kent and A. Zunger, *Appl. Phys. Lett.* **79**, 1977 (2001).
7. S. F. Chichibu, A. Uedono, T. Onuma, B. A. Haskell, A. Chakraborty, T. Koyama, P. T. Fini, S. Keller, S. P. DenBaars, J. S. Speck, U. K. Mishra, S. Nakamura, S. Yamaguchi, S. Kamiyama, H. Amano, I. Akasaki, J. Han, and T. Sota, *Nature Mater.* **5**, 810 (2006).
8. K. Fujito, S. Kubo, H. Nagaoka, T. Mochizuki, H. Namita, and S. Nagao, *J. Cryst. Growth* **311**, 3011 (2009).
9. K. Fujito, K. Kiyomi, T. Mochizuki, H. Oota, H. Namita, S. Nagao, and I. Fujimura, *Phys. Status Solidi A* **205**, 1056 (2008).
10. S. F. Chichibu, A. Uedono, T. Onuma, T. Sota, B. A. Haskell, S. P. DenBaars, J. S. Speck, and S. Nakamura, *Appl. Phys. Lett.* **86**, 021914 (2005).
11. S. F. Chichibu, K. Hazu, Y. Ishikawa, M. Tashiro, H. Namita, S. Nagao, K. Fujito, and A. Uedono, *J. Appl. Phys.* **111**, 103518 (2012).
12. M. Merano, S. Collin, P. Renucci, M. Gatri, S. Sonderegger, A. Crottini, J. D. Ganière, and B. Deveaud, *Rev. Sci. Instrum.* **76**, 085108 (2005).
13. M. Merano, S. Sonderegger, A. Crottini, S. Collin, P. Renucci, E. Pelucchi, A. Malko, M. H. Baier, E. Kapon, B. Deveaud, J. D. Ganière, *Nature* **438**, 479 (2005).
14. P. Corfdir, P. Lefebvre, J. Levrat, A. Dussaigne, J. -D. Ganière, D. Martin, J. Ristić, T. Zhu, N. Grandjean, and B. Deveaud-Plèdran, *J. Appl. Phys.* **105**, 043102 (2009).
15. S. F. Chichibu, T. Onuma, K. Hazu, and A. Uedono, *Appl. Phys. Lett.* **97**, 201904 (2010).
16. M. Kagaya, P. Corfdir, J. -D. Ganière, B. Deveaud-Plèdran, N. Grandjean, and S. F. Chichibu, *Jpn. J. Appl. Phys.* **50**, 111002 (2011).
17. T. Onuma, Y. Kagamitani, K. Hazu, T. Ishiguro, T. Fukuda, and S. F. Chichibu, *Rev. Sci. Instrum.* **83**, 043905 (2012).
18. Y. Ishikawa, M. Tashiro, K. Hazu, K. Furusawa, H. Namita, S. Nagao, K. Fujito, and S. F. Chichibu, *Appl. Phys. Lett.* **101**, 212106 (2012).
19. C. G. Dunn and E. F. Koch, *Acta Metal.* **5**, 548 (1957).
20. A. Uedono, S. Ishibashi, T. Ohdaira, and R. Suzuki, *J. Cryst. Growth* **311**, 3075 (2009).
21. K. Kumakura, T. Makimoto, N. Kobayashi, T. Hashizume, T. Fukui, and H. Hasegawa, *Appl. Phys. Lett.* **86**, 052105 (2005).
22. C. A. Klein, *J. Appl. Phys.* **39**, 2029 (1968).
23. D. Takamizu, Y. Nishimoto, S. Akasaka, H. Yuji, K. Tamura, K. Nakahara, T. Onuma, T. Tanabe, H. Takasu, M. Kawasaki, and S. F. Chichibu, *J. Appl. Phys.* **103**, 063502 (2008).